Title

Expanding the Paradigm: The influence of climate and lithology on soil phosphorus

Permalink

https://escholarship.org/uc/item/72g2w5t9

Authors

Wilson, Stewart G
Dahlgren, Randy A
Margenot, Andrew J
et al.

Publication Date

2022-09-01

DOI

10.1016/j.geoderma.2022.115809

Peer reviewed
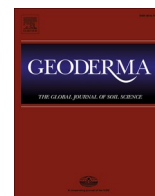
Expanding the Paradigm: The influence of climate and lithology on soil phosphorus

Stewart G. Wilson [a,*], Randy A. Dahlgren [b], Andrew J. Margenot [c], Craig Rasmussen [d], Anthony T. O'Geen [b]

[a] *Department of Natural Resources Management and Environmental Sciences, California Polytechnic State University, San Luis Obispo, CA 93407, USA*
[b] *Department of Land, Air and Water Resources, University of California, Davis, CA 95616, USA*
[c] *Department of Crop Sciences, University of Illinois Urbana-Champaign, Urbana, IL 61801, USA*
[d] *Department of Environmental Science, The University of Arizona, Tucson, AZ 85721, USA*

A B S T R A C T

The fate of phosphorus (P) during pedogenesis has been historically conceptualized (Walker-Syers model) with time as the primary controlling state factor. Herein, we demonstrate that both climate and lithology exert a strong and interacting influence on the fate of P by examining coupled bioclimatic and parent material effects on soil P fractions. Three transects were investigated spanning a 2150-m elevation gradient (MAT = 17 → 3 °C/ MAP = 330 → 1400 mm) across three separate bedrock lithologies (lithosequence: granite, andesite and basalt) within the Sierra Nevada and southern Cascades of California. The elevation gradient entails four bioclimatic zones (bioclimosequence: blue oak, ponderosa pine, white fir and red fir). Soil P fractions were determined by sequential fractionation and interpreted in the context of associated soil characterization data. The bioclimatic sequences demonstrate a weathering gradient with maximum intensity at mid-elevation sites, and corresponding changes in Fe/Al-(hydr)oxide content and aluminosilicate crystallinity. Phosphorus content of parent material varied by an order of magnitude (mean; mg P kg^{-1}): andesite (1500) > basalt (1000) > granite (131). Differences in P content of parent material influenced P_t in soils. However, amounts and proportions of P in fractions were influenced by subtle to significant interactions between climate and lithology, owing to differences in chemical weathering and the abundance and crystallinity of Fe/Al-(hydr)oxides and aluminosilicates. This interactive effect of pedogenesis on clay mineralogy led to differences in P fractions dependent upon lithology and bioclimatic zone. Labile inorganic P (P_i) was uniformly higher in soils derived from granite, despite granite having significantly lower P content, a result of lower Fe/Al-(hydr)oxide generation in granitic soils. With descending elevation and increased weathering intensity, HCl-P_i (primary mineral bound P-apatite) declined in basalt and andesite but remained unchanged in granite owing to its greater resistance to chemical weathering. As weathering intensity increased, occluded P increased in basalt, decreased in andesite and was unchanged in granite, contradicting the paradigm of progressive P occlusion with increased weathering. This incongruity for andesite results from a dominance of poorly crystalline materials (*e.g.,* ferrihydrite, allophane/imogolite) at less weathered sites versus more crystalline minerals at more weathered sites. This study highlights several caveats to the paradigm that time (*i.e.,* degree of weathering) is universally the dominant pedogenic control of P fractionation. We identify the importance of interactions between lithology and climate in regulating the amount and types of weathering products that in turn control P fractionation and ecosystem P availability.

1. Introduction

Climate and lithology are master variables of pedogenesis, yet their role in P biogeochemistry has received relatively little attention (Porder and Ramachandran, 2013; Delgado-Baquerizo et al., 2020). In the classic Walker-Syers model, the effect of time produces a trajectory of progressive P limitation and occlusion (Walker and Syers, 1976). Parent material effects are largely considered secondary to time, despite the
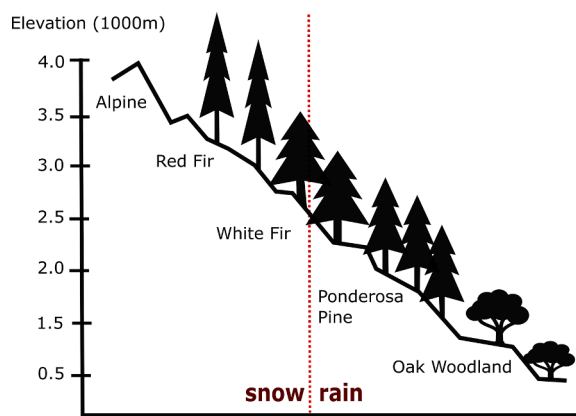
Fig. 1. Representation of elevational transects in three contrasting bedrock lithologies crossing four bioclimatic zones, adapted from Rasmussen et al. (2018). Red drop line indicates change in dominant form of precipitation (snow vs. rain). (For interpretation of the references to colour in this figure legend, the reader is referred to the web version of this article.)

fact that all terrestrial ecosystem P is ultimately rock derived (Walker and Syers, 1976; Jenny, 1994; Porder and Ramachandran, 2013; Augusto et al., 2017; Mehmood et al., 2018; Delgado-Baquerizo et al., 2020). We posit that differences in lithology and climate directly influence the evolution of soil properties and mineralogy, thereby having a distinguishing effect on soil P dynamics. Most evaluations of pedogenic state factors on P forms are based on chronosequences, none more influential than Walker and Syers (1976). Therein, total P (P_t), available P and primary mineral P, presumably apatite (Ca-Pi), declined with time, while P occluded in metal oxides and organic forms increased. The authors allude to the impact of parent material, suggesting that soils in mafic (basalt) parent materials may have a greater proportion of occluded P, due to more Fe/Al-(hydr)oxides compared to felsic (granite) materials (Walker and Syers, 1976). In spite of this recognition, limited work has followed to directly evaluate the effects of lithology on P dynamics (Mage and Porder, 2013; Porder and Ramachandran, 2013; Augusto et al., 2017; Mehmood et al., 2018; Delgado-Baquerizo et al., 2020). While previous work has highlighted the effect of parent material P on P_t in soils, we suggest that it is not simply the absolute P content of the parent material that affects the distribution of P forms in resulting soils, but rather the integrated effect of pedogenic state factors which influence the relative amounts of Fe/Al-(hydr)oxides and clay mineralogical assemblages that conspire to influence the distribution of P forms.

Results from a Hawaiian basalt chronosequence (4-million years) indicated that P_t values did not decline with time, but rather increased with weathering and peaked in 150,000 year old soils, owing to differences in the P content of lithology (Crews et al., 1995; Porder and Ramachandran, 2013). This contrasts with the Franz-Joseph chronosequence in New Zealand, where P_t declined asymptotically with time (Walker and Syers, 1976). Furthermore, non-occluded P remained elevated across the Hawaii chronosequence, but was nearly exhausted after 22,000 years in the Franz-Joseph chronosequence. The persistence of Fe/Al-(hydr)oxides in mafic soils, such as in the Hawaiian chronosequence, may increase P retention via occlusion, and hence reduce ecosystem export of P_t. Conversely, in a granitic chronosequence, all P forms declined with time, and occluded P did not increase (Adams and Walker, 1975). The lack of an increase in occluded P in soils developed from granite may result from their low Fe concentration and consequently low Fe-(hydr)oxide contents that drive P occlusion. In the Cooloola Dune chronosequence, the pre-weathered nature of the quartzose dune parent material modulated expected trends in P transformations with pedogenesis (Chen et al., 2015). Across an arid basaltic chronosequence, Ca-Pi remained elevated even after 3-million years of pedogenesis (Selmants and Hart, 2010). They concluded that climate

drove a two-order of magnitude difference in weathering rates between their arid Arizona chronosequence and the humid tropical Hawaii chronosequence (Crews et al., 1995). These climate and parent material induced differences in the trajectory of P transformations with pedogenesis highlight the need to account for the effects of diverse parent materials and climates on forms and availability of soil P.

Lithology is the single most important factor in the global distribution of soil P, exceeding climate and weathering (Augusto et al., 2017). Lithology impacts soil P dynamics directly through the total amount of P in parent material, and indirectly via the amount and forms of Fe/Al-(hydr)oxides (Dieter et al., 2010; Mage and Porder, 2013; Porder and Ramachandran, 2013; Wilson et al., 2017). Significant differences in P content of parent materials (*e.g.,* 493 vs. 1304 mg P kg^{-1} in rhyolite vs. basalt) led Porder and Ramachandran (2013) to conclude that parent material P is an explicit, yet overlooked, driver of ecosystem P. However, there are few empirical evaluations of this purported effect of parent material on soil P dynamics. In Panama, Dieter et al. (2010) found that Ca-Pi was higher in soils formed in marine sediments whereas P_t and occluded P were much higher in soils formed in andesite. Further, very high concentrations of P_t were found in soils derived from andesite, despite being in advanced weathering stages (*e.g.,* Oxisols), similar to the Hawaiian chronosequences (Crews et al., 1995). Increased P_t following intense weathering contradicts the idea of an asymptotical decline of P_t in the Walker and Syers model. Mage and Porder (2013) investigated parent material and topographic impacts on P_t, P fractions and P losses relative to parent material. They found strong parent material effects in most P metrics, even in strongly weathered soil profiles up to 10-m thick, suggesting that differences in parent material Fe content influenced P amounts/forms. Moreover, differences in initial parent material composition, especially Fe, lead to Fe-(hydr)oxide contents varying three-fold in similarly weathered soils formed from rhyolite versus basalt (Wilson et al., 2017). Large differences in lithology may contribute to differences in organic P (P_o) even in highly weathered soils (Turner and Engelbrecht, 2011). In an investigation of phosphatases that catalyze hydrolysis of organic P across three elevational transects in three bedrock lithologies, Gu et al. (2020a) noted distinct relationships between phosphodiesterase/phosphomonoesterase activities and soil properties, dependent upon lithology. Further, across 16 chronosequences, lithology was a greater driver of P_t then soil age (Delgado-Baquerizo et al., 2020). These findings collectively point to a greater impact of lithology on P dynamics than previously ascribed by Walker and Syers (1976).

To investigate the influence of climate and lithology on soil P dynamics, we studied three bioclimo-lithosequences across the Sierra Nevada and southern Cascades in California. Three transects (Δ2150-m elevation) with distinct bedrock lithologies (granite, andesite and basalt) encompassed four bioclimatic zones and incorporated consistent trajectories in the degree of weathering/pedogenesis across lithologies (Dahlgren et al., 1997b; Rasmussen et al., 2006; Rasmussen et al., 2007; Rasmussen and Tabor, 2007; Rasmussen et al., 2010). These transects offer a space for climate substitution, with a significant range in temperature (MAT = 17 to 3 °C) and precipitation (MAP = 330 to 1400 mm) known to drive differences in pedogenesis. These elevational transects enabled investigation of how changes in climate and parent material interact to regulate soil P biogeochemistry. The primary objective of this study was to expand existing paradigms of pedogenic impacts on P dynamics by explicitly integrating climate and lithology into the concept of P transformations with pedogenesis. We hypothesize that parent material and climate, integrated through pedogenic effects on weathering and mineralogy, influence the magnitude and distribution of soil P forms.

Table 1
Site descriptions and soil classification for each transect.

Ecosystem	Lithology	Elevation (m)	MAP[a] (mm yr^{-1})	MAT[b] (C)	Dominant Precipitation	Soil Classification (family)[c]	Longitude	Latitude
Red fir (*Abies magnifica*)	Basalt	2300	1340	6.5	snow	Sandy-skeletal, mixed, frigid Vitrandic Xerorthent	−121.382667	40.586417
White fir (*Abies concolor*)	Basalt	1600	1150	8.3	snow	Medial-skeletal, amorphic, mesic Typic Haploxerand	−121.6234	40.535383
Ponderosa pine (*Pinus ponderosa*)	Basalt	920	990	14.2	rain	Fine, parasesquic, mesic Xeric Palehumult	−121.921467	40.5005
Blue oak (*Quercus douglasii*)	Basalt	280	780	16.7	rain	Fine-loamy, mixed, superactive thermic Ultic Haploxeralf	−122.0965	40.464017
Red fir (*Abies magnifica*)	Andesite	2150	1350	6	snow	Medial-skeletal, amorphic, frigid Humic Vitrixerand	−120.225217	38.628367
White fir (*Abies concolor*)	Andesite	1700	1400	8.5	snow	Medial-skeletal, amorphic, mesic Humic Haploxerand	−120.397983	38.698467
Ponderosa pine (*Pinus ponderosa*)	Andesite	1150	1250	11.5	rain	Clayey-skeletal, mixed, active, mesic Ultic Haploxeralf	−120.550133	38.710133
Blue oak (*Quercus douglasii*)	Andesite	160	460	17	rain	loamy-skeletal, mixed, superactive thermic Lithic Ultic Haploxeroll	−120.76645	38.386917
Red fir (*Abies magnifica*)	Granite	2195	1080	7.2	snow	Loamy-skeletal, mixed, frigid Dystric Xerochrepts	−119.1995	37.162517
White fir (*Abies concolor*)	Granite	1800	1010	9.1	snow	Sandy, mixed, mesic Pachic Xerumbrept	−119.14595	37.054933
Ponderosa pine (*Pinus ponderosa*)	Granite	1390	910	11.1	rain	Fine-loamy, mixed, semiactive, mesic Ultic Haploxeralf	−119.372283	37.061217
Blue oak (*Quercus douglasii*)	Granite	198	330	16.7	rain	Coarse-loamy, mixed, thermic Typic Xerochrept	−119.477183	37.081867

[a] mean annual precipitation, [b]mean annual temperature, [c]adapted from Dahlgren et al., 1997b; Rasmussen et al., 2006; Rasmussen et al., 2007; Rasmussen et al., 2010.

2. Methods

2.1. Site description

This investigation included twelve sites representing three parent materials (granite, andesite, basalt) across an elevation gradient spanning four bioclimatic zones defined by dominant tree species and position along transect, blue oak; lowest elevation (*Quercus douglasii*; OK-1), ponderosa pine; mid-lower elevation (*Pinus ponderosa*; PP-2), white fir; mid-higher elevation (*Abies concolor*; WF-3), and red fir; highest elevation (*Abies magnifica*; RF-4) (Fig. 1). Vegetation and distinct ecoregions on the western slope of the Sierra Nevada and southern Cascade ranges is tightly tied to elevation by virtue of climatic differences (Griffith et al., 2016; O'Geen et al., 2018). Bioclimatic zones become drier and warmer with decreasing elevation (Table 1). Precipitation occurs dominantly as rain at lower elevations (OK-1, PP-2) and as snow at higher elevations (WF-3, RF-4); climate is Mediterranean with the majority of precipitation occurring in the winter season (November – March). Given that most of the precipitation falls when dominant tree species are dormant, we assume that the effective depth of precipitation largely follows trends of precipitation (O'Geen et al., 2018). While the highest elevation granite, andesite and basalt sites sit outside the extent of Pleistocene glaciation, they were likely influenced by periglacial processes (Holbrook et al., 2014; Turrin et al., 1998; Gillespie and Zehfuss, 2004). However, while we cannot discount periglacial influences at our highest elevation sites, we assume that these effects are similar across sites and that the soils therein have integrated weathering from glacial and interglacial periods (Holbrook et al., 2014). The elevational transects in this investigation have proven useful to quantify the influence of climate

on soil formation, soil properties and nutrient cycling (Jenny, 1994; Southard and Southard, 1987; 1989; Alexander et al., 1993; Takahashi et al., 1993; Dahlgren et al., 1997b; Takahashi et al., 2001; Rasmussen et al., 2007; Rasmussen et al., 2010 and others).

2.2. Soil and rock sampling

Pedons were selected from stable landforms (shoulder hillslope position) with slopes ranging from 10 to 15%. Three pedons were sampled from each of the 12 sites (3 lithologies × 4 bioclimatic zones). Pedons were excavated to refusal or to at least 200 cm for deeper pedons. Soils were sampled by genetic horizon, air-dried and sieved to pass a 2-mm screen. Soil samples for andesite and basalt transects were archived samples from previous studies (Rasmussen et al. 2007, Rasmussen et al. 2010). Readers are directed to Dahlgren et al., 1997a, Rasmussen et al., 2007 and Rasmussen et al., 2010 for general soil characterization data. Rock samples were obtained from the bottom of soil pits, or from a nearby road cut in the case of deeply weathered profiles. Underlying bedrock consists of andesitic lahar material from late Miocene to Pliocene age from the Mehrten formation, basalt flows from the mid to late Pleistocene, and the granite batholith of the Sierra Nevada thought to be Eocene in age (Piper et al., 1939; Mix et al., 2016). Regolith residence times calculated from cosmogenic nucleotides for the granite sites are thought to be <100,000 years (Riebe and Granger, 2013). We assume that soil and regolith production at the rock soil interface is in steady state with late Holocene denudation rates (Holbrook et al., 2014). Overall, the net effect of pedogenic processes within a site are in equilibrium with the dynamics of soil forming factors at the location (Buol et al., 2011). Therefore, within a lithosequence (*i.e.,* different lithologies

Table 2
Total elemental analysis of parent materials across a bioclimatic gradient (mean $\pm$ SE)[1].

Lithology	Biome	P_2O_5	Na_2O	CaO	K_2O	MgO	Al_2O_3	SiO_2	Fe_2O_3
		mass %							
Basalt	Red fir	0.18^b (0.03)	3.2^{ab} (0.1)	6.2^a (0.1)	1.5^b (0.2)	3.4^a (<0.1)	19.1^a (0.7)	57.0^b (0.9)	6.4b (0.2)
Andesite	Red fir	0.28^a (0.01)	3.3^a (0.1)	7.0^a (0.7)	1.9^b (0.2)	4.0^a (0.3)	18.3^a (0.2)	54.4^b (1.2)	7.9^a (0.5)
Granite	Red fir	0.03^c (<0.01)	2.8^b (<0.1)	1.2^b(<0.1)	5.00^a (0.3)	0.2^b(<0.1)	13.7^b (0.5)	74.5^a (0.8)	1.5^c (0.2)
Basalt	White fir	0.25^b (0.02)	2.8 (0.1)	8.0^a (0.4)	0.4^b (<0.1)	6.8^a (0.2	18.9^a (0.5)	51.7^b (1.4)	7.4^a (0.2)
Andesite	White fir	0.36^a (0.02)	2.8 (0.2)	7.4^a (0.9)	1.1^b (0.2)	4.5^b (0.8)	20.1^a (0.7)	49.9^b (2.1)	9.1^a (0.8)
Granite	White fir	0.02^c (<0.01)	2.4 (0.3)	1.1^b (0.3)	5.0^a (0.5)	0.1^c (<0.1)	13.8^b (0.7)	74.6^a (0.8)	1.4^b (0.5)
Basalt	P. Pine	0.19^b (<0.01)	3.1^b (<0.1)	7.6^a (0.3)	1.3^b (<0.1)	5.5^a (0.2)	16.8^b (0.5)	55.4^b (0.5)	7.9^a (<0.1)
Andesite	P. Pine	0.3^a (0.01)	3.9^a (<0.1)	6.6^a (0.2)	2.1^a (0.1)	2.9^b (0.2)	18.7^a (0.1)	57.5^{ab} (0.6)	6.2^a (0.2)
Granite	P. Pine	0.18^b (0.02)	2.9^b (0.2)	4.8^b (0.7)	2.1^a (0.1)	2.4^b (0.5)	17.1^b (0.2)	61.6^a (2.1)	5.8^a (1.0
Basalt	Oak	0.12^b (<0.01)	2.4^b (<0.1)	10.8^a (0.2)	0.2^b (<0.1)	9.3^a (<0.1)	17.1^b (<0.1)	47.8^c (0.2)	10.6^a (<0.1)
Andesite	Oak	0.26^a (0.02)	3.7^a (0.2)	6.4^b (0.2)	1.1^a (0.2)	3.3^b (0.3)	19.1^a (0.6)	57.00^b (0.3)	6.6^b (0.3)
Granite	Oak	0.03^c (<0.01)	4.1^a (0.2)	2.6^c (0.1)	1.4^a (<0.1)	0.5^c (<0.1)	16.2^b (0.3)	70.8^a (1.1)	2.0^c (0.2)

[1] Within a biome, means with different letters are significantly different at $p < 0.05$ by Tukey's HSD.

in the same bioclimatic zone) we assume that differences in soil properties (*e.g.,* soil depth, weathering rates, P fractions) are largely driven by differences in lithology. Similarly, differences in soil depth and degree of weathering between lithologies in a common climate are an expression of the differences in chemical and physical weathering rates among rock types. For example, granite largely physically weathers via expansion of biotite and physical breaking of rock (Wahrhaftig, 1965) leading to deeper but less chemically altered soils, whereas basalt weathers chemically relatively rapidly (Zhang et al., 2007), albeit to a relatively shallow depth (Pillans, 1997).

2.3. Total elemental analysis of rock and soil

Any surficial-rock weathering rind was removed with a lapidary slab saw. The resulting unweathered interior rock sample was treated with 5% hydrogen peroxide solution for 24 h to remove surficial organic matter, then dried and crushed. Rock ($n = 36$) and soil ($n = 156$) samples were pulverized with a carbide-steel shatter box to pass a 74-μm sieve. Total elemental analysis (Al, Ca, Fe, K, Mg, Na, P and Si) was determined on ground samples using lithium borate fusion with quantification via X-ray fluorescence (XRF) spectroscopy by ALS-Geochemistry (Sparks, NV) and reported as major oxides. A basalt reference standard was used, with P recovery of 99-/+% (NIST-SRM 688).

2.4. Hedley fractionation

The modified Hedley fractionation procedure was used to quantify P into operationally defined pools (Hedley et al., 1982; Tiessen and Moir, 1993). Sequential extractions to operationally define P fractions have been used to approximate biogeochemical P pools that change with soil weathering (Walker and Syers, 1976; Tiessen et al., 1984; Tiessen and Moir, 1993). The use of chemical solubility of P as proxy of speciation and availability has been rightfully questioned (Klotzbücher et al., 2019; Gu et al., 2020b). Fractionation of mineral P standards have shown that common interpretations of fractions as pools are not necessarily valid and in some cases may entail a serious degree of misinterpretation (Barrow et al., 2021). On the other hand, some P fractions have a clear interpretation as specific P pools sensitive to soil-forming factors, in particular anion exchangeable resin extractable P and organic P fractions (Gu and Margenot, 2021). Depending on soil mineralogy, HCl-P_i can also provide highly accurate estimates of apatite P, as confirmed by K-edge X-ray absorption near-edge structure (XANES) (Gu et al., 2020b). Meta-analyses of P fractions broadly corroborate soil P bioavailability (Tiessen et al., 1984; Hou et al., 2016; Nakayama et al., 2021) and biogeochemical models (Cross and Schlesinger, 1995; Yang and Post, 2011). Sequential fractionations can also offer more information on P pools such as organic P (Gu and Margenot, 2021) and apatite

(Helfenstein et al., 2018) than XANES. Thus, soil P fractions are operationally interpreted in the present work as proxies for pools reflective of P transformations during pedogenesis.

Briefly, duplicate 1-g soil samples were sequentially extracted with $NaHCO_3$-saturated anion exchange resin-membrane (1 $\times$ 4 cm, VWR International, West Chester, PA), and 20 ml of 0.5 M $NaHCO_3$, 0.1 M NaOH, and 1 M HCl in 50-mL polypropylene tubes. Samples were shaken for 18 h and extracts isolated by centrifugation followed by analysis for reactive P_i using the ammonium molybdate-ascorbic acid method (Murphy and Riley, 1962). Total P (P_t) in $NaHCO_3$ and NaOH extracts was determined following digestion in 0.9 M H_2SO_4 and $(NH_4)_2S_2O_8$, and organic P (P_o) was determined as the difference between digested and undigested samples. P_t was determined by lithium-borate fusion and XRF spectroscopy as described above. Occluded P, which is residual P not solubilized in the Hedley fractionation, was determined as the difference between P_t and the sum of P fractions extracted ($P_{occluded} = P_{total}-P_{sum\ of\ fractions}$) (Crews et al., 1995). While HCl-P_i is often interpreted as Ca-P_i, and NaOH-P_i as Fe/Al associated P_i, we present P fractions via extracting solution, with the following exceptions: labile-P_i (Resin + $NaHCO_3$ P_i), occluded P ($P_{occluded} = P_{total}-P_{sum\ of\ fractions}$) and total P_o ($P_o = NaHCO_3\ P_o + NaOH\ P_o$). Concentrations (mg kg^{-1}) were reported as a depth weighted mean for the solum (A + B horizons).

2.5. Selective dissolution and measures of chemical weathering

Non-sequential selective dissolution in acid ammonium-oxalate (Burt and Staff, 2014) and citrate-dithionite (Holmgren, 1967) was used to characterize pedogenic pools of Fe and Al. Oxalate extractable Al (Al_o) and Fe (Fe_o) originate from organic complexes, poorly crystalline Fe-(hydr)oxides (*e.g.,* ferrihydrite) and allophane/imogolite. Citrate-dithionite extractable Fe (Fe_d) originates from organic complexes and both poorly crystalline and crystalline Fe-(hydr)oxides. Al concentrations in all extracts were determined via atomic absorption spectroscopy, and Fe concentrations via ferrozine colorimetry (Stookey, 1970). Total Fe (Fe_t) was determined by lithium-borate fusion and XRF spectroscopy as described above. The crystalline Fe fraction was calculated as the difference between Fe_d and Fe_o (crystalline Fe = Fe_d-Fe_o). Chemical weathering was assessed by two methods. First, the ratio of Fe_d/Fe_t (termed degree of weathering herein) was calculated as the fraction of iron released from primary minerals by weathering. Second, the chemical index of alteration (CIA) was calculated for soils, which uses oxide values converted to molar values calculated as: CIA = $[Al_2O_3/(Al_2O_3 + Na_2O + CaO + K_2O)] \times 100$. Weathering products such as kaolinite have CIA values ≈ 100, whereas fresh basalts and granites have a CIA between 30 and 45 and 45–55, respectively (Nesbitt and Young, 1982).
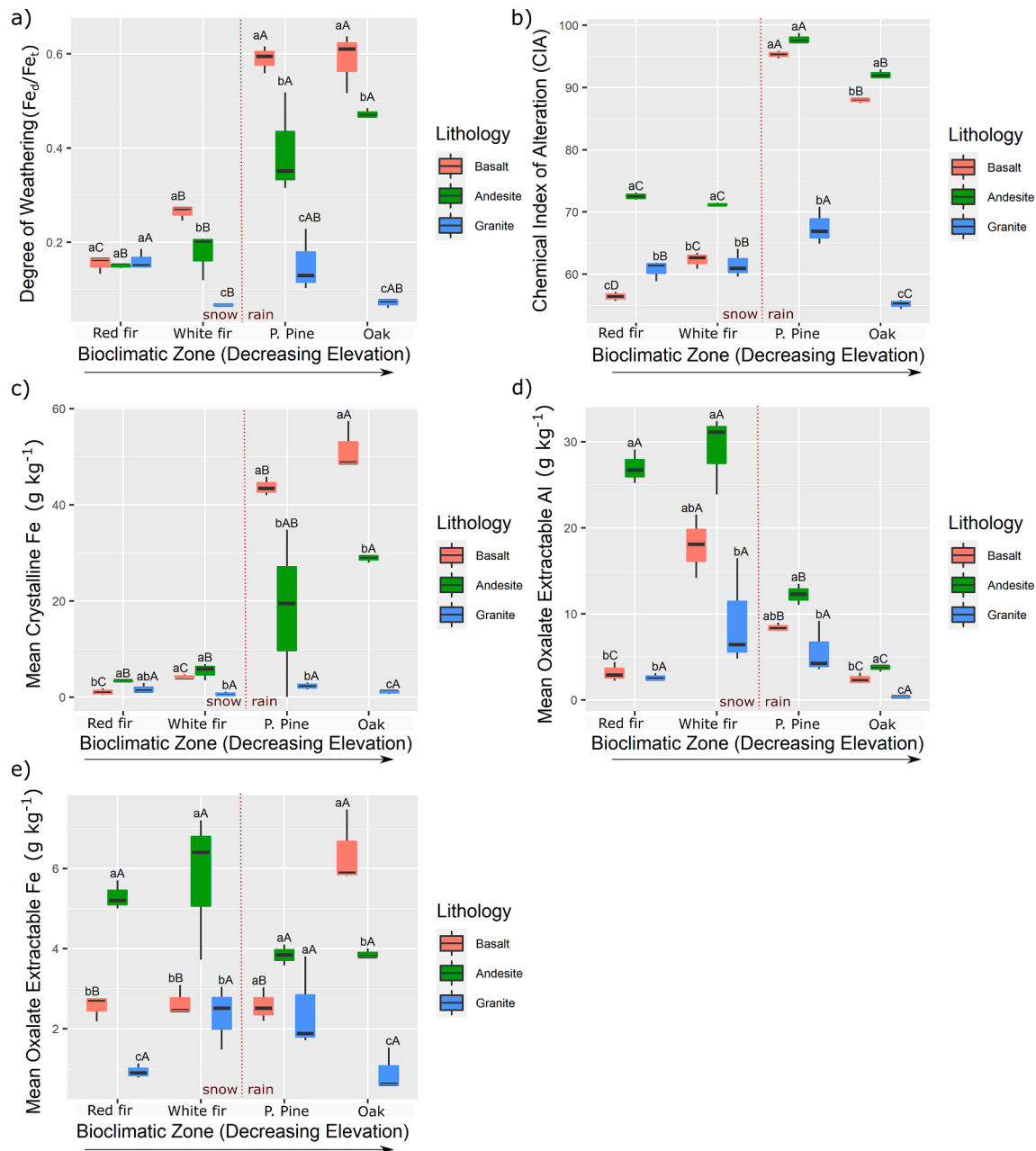
Fig. 2. Box plots of depth weighted mean for a) degree of weathering (ratio of Fe_d/Fe_t), b) chemical index of alteration (CIA), c) crystalline Fe (Fe_d-Fe_o), d) oxalate extractable Al (Al_o) and e) oxalate extractable Fe (Fe_o) in solum (A and B horizons combined) for each lithology and bioclimatic zone. Lowercase letters show significant differences ($p < 0.05$) between lithologies within a bioclimatic zone. Upper case letters show significant differences ($p < 0.05$) between bioclimatic zones for lithology. Bars are minimum and maximum values; red drop line indicates change in dominant form of precipitation (snow vs. rain). (For interpretation of the references to colour in this figure legend, the reader is referred to the web version of this article.)

2.6. Data presentation and statistical analysis

To make comparisons between equivalent pedogenic horizons, depth-weighted averages in mg P per kg soil for the solum (A and B horizons) were used among parent materials and bioclimatic zones. To identify significant differences between combinations of lithology and bioclimatic zone, analysis of variance (ANOVA) was performed with concentrations of solum P fractions as the response variable, and lithology and bioclimatic zone as explanatory variables. Initial exploratory analysis revealed significant interactions in main effects (bioclimate × lithology), necessitating analysis of simple effects for individual lithology and bioclimatic zones by one-way ANOVA. When significant simple effects ($p < 0.05$) were determined, mean separation

followed to identify differences among bioclimatic zones or lithologies via Tukey's HSD. When ANOVA assumptions (*e.g.* normality of residuals or homogeneity of variance) failed, log or square root transformations were applied to meet assumptions. Assumptions of normality of residuals for crystalline Fe were not met following data transformation. As a result, the Kruskal-Wallis test for non-normal data was used rather than one-way ANOVA. To further elucidate the influence of climate and lithology on P fractions, P fractions were normalized to P_t and reported as proportions of P_t.

To test relationships among lithology, climate, pedogenic Fe/Al, measures of chemical weathering and P fractions, data were analyzed via conditional inference trees (CIT). CIT are a tree based, non-parametric regression method with nodes based on a p-value, instead
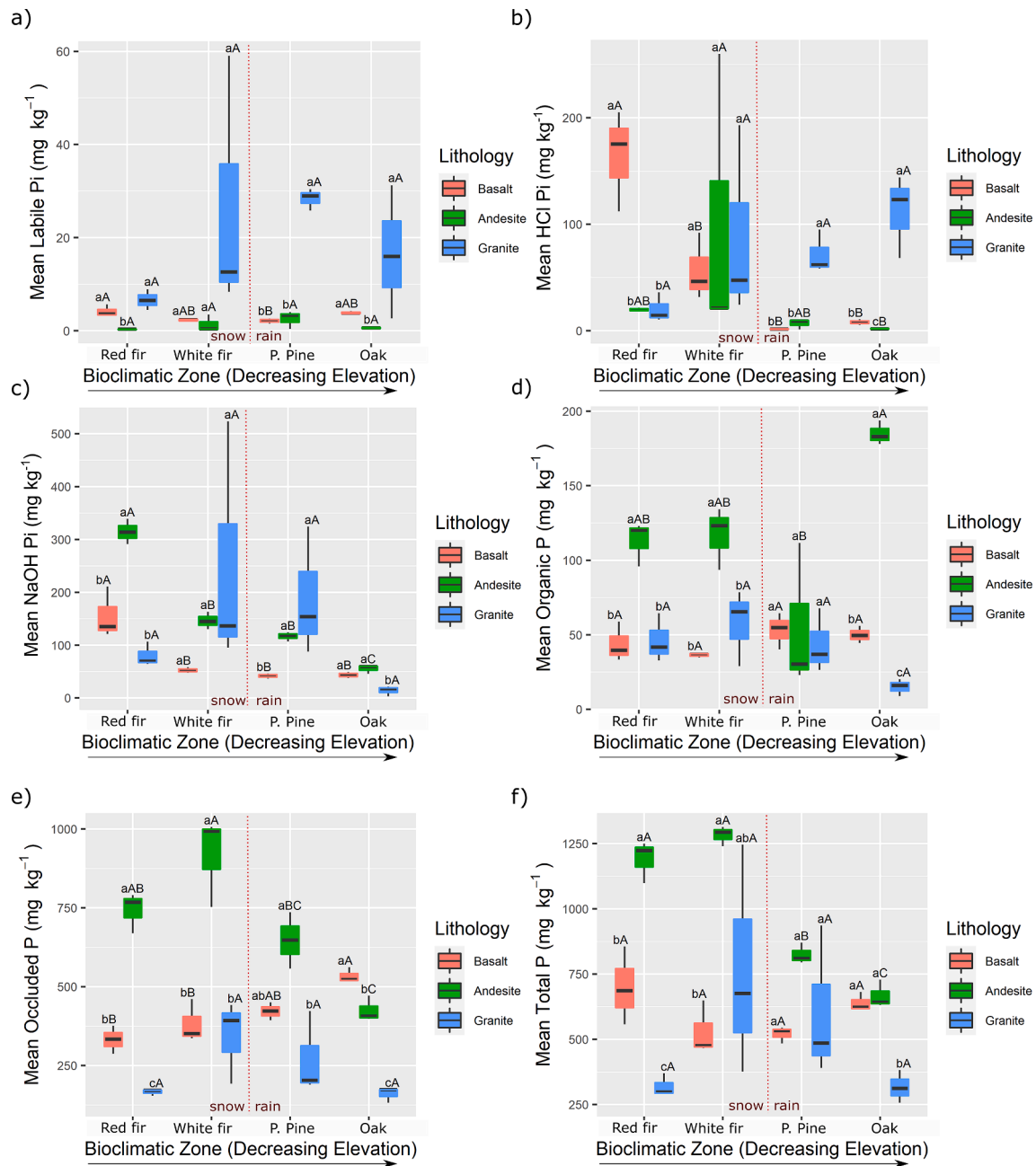
Fig. 3. Box plots of depth weighted mean for: a) Labile P_i, b) HCl-P_i, c) Organic P, d) NaOH-P_i, e) Occluded P and F) Total P in solum (A and B horizons) for each lithology and bioclimatic zone. Lower case letters show significant differences ($p < 0.05$) in P fractions between lithologies within a bioclimatic zone. Upper case letters show significant differences ($p < 0.05$) in P fractions between bioclimatic zones for a lithology. Bars are standard minimum and maximum values.

of a reduction in the sum of squared errors (Hothorn et al., 2006). CIT was created specifically to guard against overfitting and bias in variable selection (Hothorn et al., 2006; Hothorn and Zeileis, 2015). In CIT, splits are made only when there exists a significant relationship between response variables and predictors. Partitioning stops when no significant association exists between covariates and the response. Since splits of the tree are only made when a significant relationship exists between the predictors and the response, the performance of CIT is similar to pruned regression trees (Hothorn et al., 2006). Initial data exploration revealed that for each lithology, different explanatory variables predicted the P fraction response. Thus, CIT allow for higher level, strong predictors (*e.g.,* lithology) to drive initial partitions of the data, with subsequent child nodes partitioned on covariates, therefore identifying underlying relationships in the data. To further elucidate the role of covariates in P

dynamics, a Pearson's correlation analysis was used to examine possible contributing effects of pedogenic Fe/Al and measures of chemical weathering to various P fractions. Due to contradictory correlations among lithologies (*e.g.,* a response and predictor exhibiting a positive correlation in one rock type and a negative correlation in a different rock type), correlations were examined for each lithology independently. All statistical analyses were performed in R using a $p < 0.05$ level of significance (R Core Team, 2020).

3. Results

3.1. Lithology

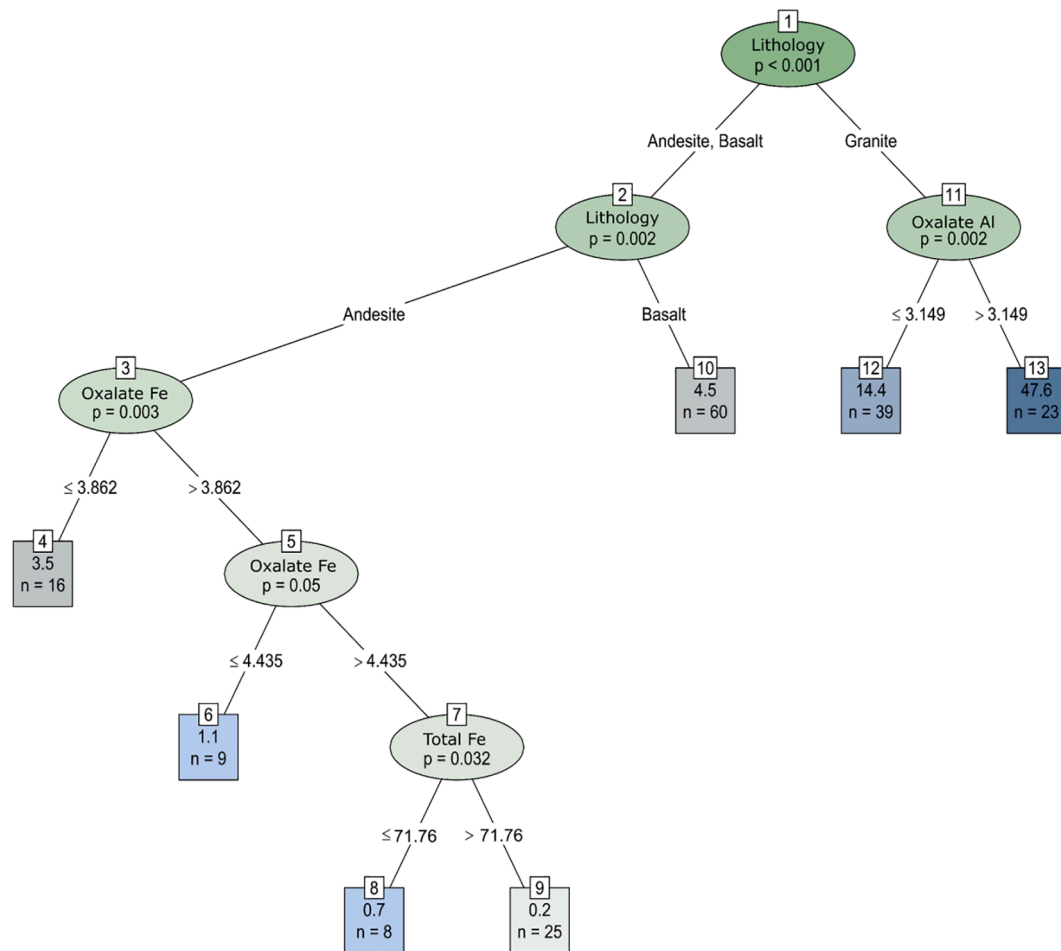Rocks from the three bedrock types followed expected trends with

Fig. 4. Conditional inference tree for labile P_i in the solum. P-values indicate a significant relationship between covariate and response in that split of the data. Numbers along branches indicate values of the predictor variable used to make the split of the data. Numbers in terminal nodes/boxes indicate number of response variable data points (n) and mean of these data points in that partition of the data space.

more mafic rocks higher in Fe_2O_3, CaO and MgO, and lower in SiO_2 and K_2O (Table 2). At all bioclimatic zones, andesite had significantly more P_2O_5 (P_t) than basalt and granite. Basalt had significantly more P_2O_5 than granite, except in the PP-2 zone, where basalt and granite rocks had similar P_2O_5 concentrations. Granite was markedly lower in P_2O_5 compared to basalt and andesite, in all bioclimatic zones except PP-2. The rock composition in the PP-2 zone of the granitic transect had a lower silica composition, characteristic of Sierran granitoid rocks, such as granodiorites (Ducea, 2001; Frost et al., 2001).

3.2. Chemical weathering and selective dissolution

With descending elevation among transects from RF-4 → WF-3 → PP-2, soils tend to become more weathered as temperature increases, yet precipitation remains relatively high. The magnitude of this weathering effect depends on lithology (Fig. 2). Descending elevation among transects, degree of weathering (Fe_d/Fe_t) and CIA tend to increase, especially across the snow to rain transition (WF-3 to PP-2) (Fig. 2a; Fig. 2b). Similarly, in basalt and andesite, amounts of crystalline Fe increased whereas poorly crystalline Fe decreased with decreasing elevation (Fig. 2c; Fig. 2d). At rain dominated sites, soils derived from basalt and andesite were relatively enriched in crystalline Fe compared to granite (Fig. 2c). Crystalline Fe increased with decreasing elevation in andesite and basalt, but not in granite (Fig. 2c). Al_o was significantly higher in andesite compared to basalt and granite, owing to the presence of allophane/imogolite (Fig. 2d). For the andesite transect, Al_o decreased with elevation, while for the basalt transect Al_o increased from RF-4 to

WF-3, then declined sharply from WF-3 to PP-2 (Fig. 2d). Fe_o was highest in andesite soils in snow dominated sites (RF-4, WF-3), and highest in basalt soils in the OK-1 bioclimatic zone (Fig. 2e). In granite, Al_o and Fe_o were not influenced by bioclimate (Fig. 2d, Fig. 2e).

3.3. Effect of climate and lithology on P dynamics

Lithology was a significant driver of the magnitude of P fractions in all bioclimatic zones, with soil P fractions differing significantly depending on fraction, bioclimate and lithology (Fig. 3). Labile P_i was higher in granite-derived soils compared to soils formed from andesite across all bioclimatic zones, and more than andesite and basalt in the PP-2 bioclimatic zone. Labile P_i was higher in soils derived from basalt compared to andesite in RF-4 and OK-1 (Fig. 3a). Climatic differences across the basalt transect influenced labile P_i, with a significant decline in labile P_i from RF-4 to PP-2 as elevation decreased and weathering increased (Fig. 3a). Labile P_i was lowest in soils of the andesite transect.

Changes in the significance of rock type with differences in bioclimatic zone were also noted in $NaOH-P_i$ (Fig. 3c). In RF-4, soils derived from andesite had significantly more $NaOH-P_i$ than those in granite and basalt. In PP-2, soils derived from andesite and granite had more $NaOH-P_i$ than basalt (Fig. 3c). These differences are due to differences in the interaction of bioclimate and lithology with respect to $NaOH-P_i$. Soils derived from basalt declined significantly from RF-4 to WF-3 and remained low from WF-3 to PP-2 and OK-1 (Fig. 3c). In andesite-derived soils, $NaOH-P_i$ consistently declined with decreasing elevation and increased weathering (Fig. 3c). In granite, $NaOH-P_i$ remained

Table 3
Pearson's correlations between labile Pi, HCl Pi, NaOH Pi, Organic P, Occluded P, Total P and measures of chemical weathering and pedogenic Fe and Al in basalt, andesite and granite transects.

Fraction	Labile Pi			HCl Pi			NaOH Pi			Organic P			Occluded P			Total P		
Lithology	Basalt	Andesite	Granite	Basalt	Andesite	Granite	Basalt	Andesite	Granite	Basalt	Andesite	Granite	Basalt	Andesite	Granite	Basalt	Andesite	Granite
Degree of Weathering (Fe_d/Fe_t)	−0.25	−0.08	−0.15	**−0.75*****	**−0.40****	**−0.26***	**−0.58*****	**−0.65*****	0.02	0.15	**0.35****	0.12	**0.59*****	**−0.55*****	0.03	−0.09	**−0.66*****	−0.03
CIA	**−0.31****	0.19	−0.08	**−0.77*****	**−0.37****	**−0.30****	**−0.57*****	**−0.59*****	0.16	0.13	−0.06	−0.01	**0.50*****	**−0.53*****	**0.33****	−0.17	**−0.70*****	0.11
Oxalate Fe	−0.01	**−0.47*****	**0.44****	−0.02	−0.07	**0.44*****	−0.03	**0.39****	**0.78*****	0.02	**0.33***	**0.55*****	**0.39****	**0.39*****	**0.80*****	**0.29****	**0.46*****	**0.78*****
Crystalline Fe	−0.23	−0.17	−0.16	**−0.72*****	**−0.38****	−0.22	**−0.54*****	**−0.64*****	−0.05	0.13	0.22	−0.2	**0.58*****	**−0.60*****	0.09	−0.08	**−0.72*****	−0.07
Total Fe (PPM)	**−0.30****	−0.09	**0.31***	**−0.66*****	**−0.39****	**0.29****	**−0.43*****	**−0.42*****	**0.48*****	0.05	−0.25	0.1	**0.54*****	**−0.61*****	**0.61*****	−0.05	**−0.73*****	**0.50*****
Oxalate Al	−0.23	−0.19	**0.47*****	0.22	0.25	**0.45*****	0.16	**0.64*****	**0.80*****	−0.18	−0.07	**0.71*****	**−0.34****	**0.63*****	**0.81*****	−0.15	**0.74*****	**0.82*****

Statistically significant correlations are highlighted in bold: $p < 0.05$, <0.01, and <0.001 are indicated by *, ** and ***respectively.

---

unchanged across the transect (Fig. 3c).

The HCl-P_i fraction highlights the influence of lithology on the magnitude of P fractions for different bioclimatic zones (Fig. 3b). For example, in the RF-4 bioclimatic zone, soils derived from basalt were significantly higher in HCl-P_i compared to soils derived from other rock types. In WF-3, all rock types were similar in HCl-P_i. In PP-2 and OK-1, soils derived from granite were significantly higher in HCl-P_i, highlighting the changing significance of lithology by bioclimatic zone (Fig. 3b). Soils derived from basalt declined significantly in HCl-P_i from RF-4 to WF-3, and trended lower in PP-2 and OK-1. Soils derived from andesite declined significantly in HCl-P_i from WF-3 to OK-1. In contrast, HCl-P_i was similar across the transect for soils derived from granite (Fig. 3b). With respect to P_o, soils derived from andesite were significantly higher in P_o than all other lithologies in all bioclimates except PP-2 and was especially high in OK-1 (Fig. 3d). Significant bioclimatic effects were not observed for P_o in granite and basalt transects (Fig. 3d).

Occluded P showed strong interactions between climate and lithology, with each rock type displaying different trends across transects (Fig. 3e). As weathering intensity increased, occluded P decreased in soils derived from andesite, declining significantly from WF-3 to PP-2 and from PP-2 to OK-1 (Fig. 3e). Conversely, in basalt soils, occluded P increased with increased weathering intensity such that the OK-1 zone had significantly more occluded P than RF-4 and WF-3 (Fig. 3e). Granitic soils were statistically similar in occluded P across the transect (Fig. 3e). Descending the transect, andesite declined in occluded P, basalt increased in occluded P, and granite was unchanged (Fig. 3e).

Soils formed from andesite generally had more P_t compared to soils formed from other rocks (Fig. 3f). In OK-1, both andesite and basalt soils had more P_t than granite. P_t declined significantly in andesite soils with increased weathering (declining elevation). Granitic soils showed a notable increase in P_t from RF-4 to WF-3, and similar P_t for WF-3 and OK-1. When fractions were reported as a percent of P_t, trends across the transects and differences between rock types were complimentary to those reported as a concentration (Figs. 10 and 11 in Appendix D).

3.4. Relationships between P fractions, measures of chemical weathering and pedogenic Fe and Al. Conditional inference tree structures and Pearson's correlation analysis.

3.4.1. Labile P_i

Conditional inference trees (CIT) and Pearson's correlation analysis suggest contrasting relationships between measures of chemical weathering, pedogenic Fe and Al, and labile P_i dependent upon lithology. Labile P_i partitioning by CIT was driven by lithology, with granite distinguished from andesite and basalt (Fig. 4). Labile P_i was further split by lithology, with basalt on one branch and andesite on another. In the andesite branch, Fe_o drove differentiation of labile P_i. Correlation analysis yielded additional inferences. For basalt, significant negative correlations were observed between labile P_i and CIA (Table 3; r = −0.31), while both andesite and granite had non-significant relationships between CIA and labile P_i. Labile P_i was negatively correlated with Fe_o in andesite (Table 3; r = −0.47) and positively in granite (Table 3; Fe_o, r = 0.44).

3.4.2. HCl-P_i

Both CIT and correlation analysis revealed strong relationships between indicators of chemical weathering and HCl-P_i. HCl-P_i was strongly associated with CIA, with the initial most significant split of data driven by CIA (Fig. 5). Fe_t inherited from parent rock and degree of weathering (Fe_d/Fe_t) were also significant splitting variables (Fig. 5). Correlation analysis revealed differences in the magnitude of correlation between indicators of chemical weathering and HCl-P_i dependent on rock type. Basalt showed the strongest negative correlation between HCl-P_i and measures of chemical weathering: Fe_d/Fe_t (Table 3; r = −0.75) and CIA (Table 3; r = −0.78). In andesite, HCl-P_i show a significant negative association with indicators of chemical weathering, Fe_d/Fe_t (Table 3; r
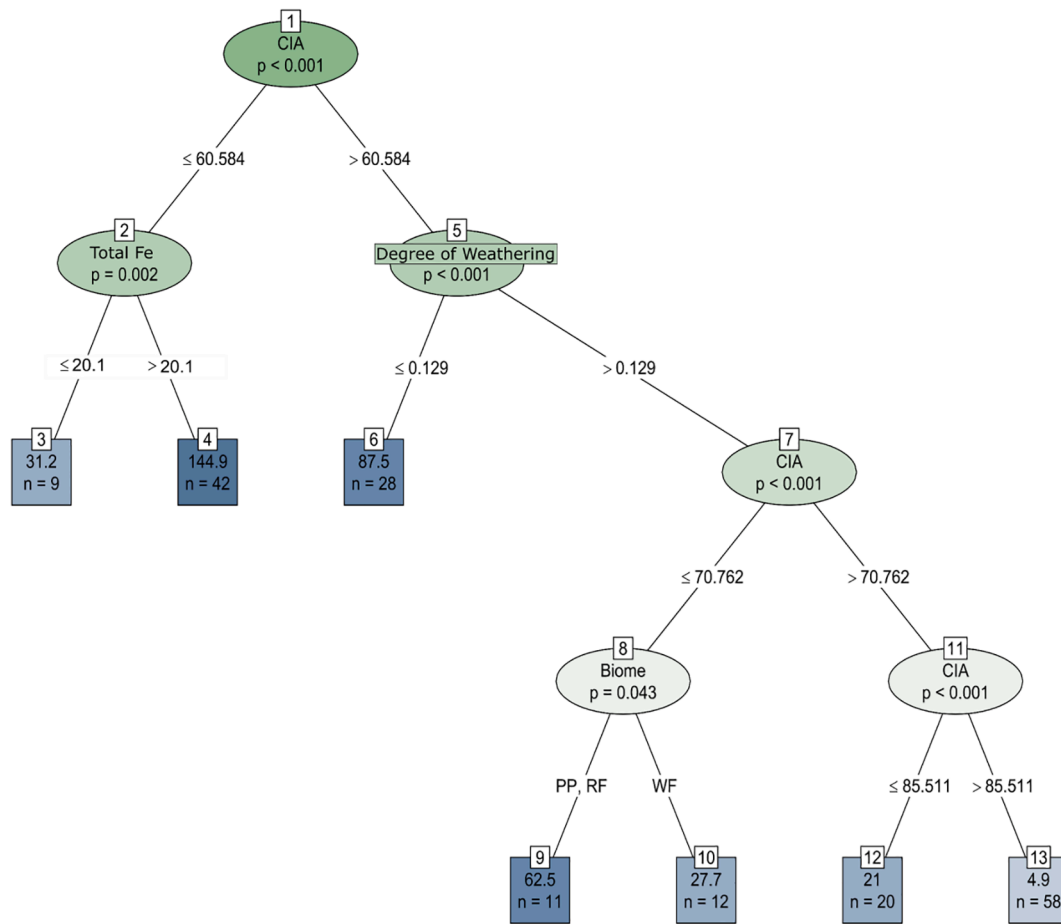
Fig. 5. Conditional inference tree for HCl-P_i in the solum. P-values indicate a significant relationship between covariate and response in that split of the data. Numbers along branches indicate values of the predictor variable used to make the data split. Numbers in terminal nodes/boxes indicate number of response variable data points (n) and mean of these data points in that partition of the data space.

= -0.40) and CIA (Table 3; r = −0.37), but to a lesser degree than basalt. Granite showed the weakest relationship between HCl-P_i and CIA (Table 3; r = −0.30) and Fe_d/Fe_t (Table 3; r = −0.26). In contrast to andesite and basalt, Fe_o was positively correlated with HCl-P_i in granite.

3.4.3. *NaOH-P_i*

CIT analysis revealed a complex set of significant covariates splitting the NaOH-P_i data (Fig. 6). Degree of weathering (Fe_d/Fe_t) was the most important covariate in partitioning NaOH-P_i. In highly weathered samples, lithology significantly defined the next branch, with andesite and granite on one branch and basalt on the other, with subsequent distinctions based on bioclimatic zone. In soils with a lower Fe_d/Fe_t, Fe_o, Fe_t and Al_o, lithology and biome were all significantly associated with NaOH-P_i. Lithology was also a significant splitting variable in soils with a low degree of weathering, and higher amounts of poorly crystalline Fe (Fe_o), with granite, andesite and basalt each on separate branches.

Dependent upon rock type, correlations between NaOH-P_i, measures of chemical weathering and pedogenic Fe and Al contrasted. For example, in both basalt and andesite transects, NAOH-P_i showed a strong negative correlation with both indices of chemical weathering (Table 3), suggesting that as weathering increased, NaOH-P_i decreased. However, in granite, no relationships were found between indicators of chemical weathering and NaOH-P_i. Further, soils formed in andesite showed strong positive correlations between NaOH-P_i and amounts of Fe_o (Table 3; r = 0.39) and Al_o (Table 3; r = 0.64), whereas no relationships were found in basalt.

3.4.4. *Organic P*

CIT analysis revealed lithology as the strongest predictor of P_o, with andesite on one branch and basalt and granite on the other (Fig. 7). This is in general agreement with the interpretation of ANVOA results (Fig. 3d), wherein andesite always had the highest levels of P_o. Within andesite lithologies, bioclimate was a strong predictor of P_o, with differentiation between PP-2, RF-4 and WF-3 driven by Fe_o concentrations. Broadly, andesitic OK-1 biomes, and conifer biomes with high Fe_o had the most P_o. In basalt, measures of chemical weathering and pedogenic Fe and Al were not correlated with P_o (Table 3). In andesite, both Fe_d/Fe_t (Table 3; r = 0.35) and Fe_o (Table 3; r = 0.33) were positively correlated with P_o. In granite, Fe_o (Table 3; r = 0.55) and Al_o (Table 3; r = 0.71) were positively correlated with P_o.

3.4.5. *Occluded P*

CIT analysis revealed that P occlusion was strongly associated with pedogenic Fe and Al (Fig. 8). The most significant variable splitting the occluded P data was Fe_o concentration, with P occlusion in soils with high Fe_o best differentiated by Al_o concentrations. Soils with both high Fe_o and Al_o had the highest occluded P. In soils with lower Fe_o, occluded P was differentiated by Fe_t, Fe_o, crystalline Fe and Al_o.

Contrasting controls on P fractions dependent on lithology were evident in correlations between occluded P, measures of chemical weathering and pedogenic Fe/Al. In basalt, the degree of chemical weathering (Table 3; r = 0.59), CIA (Table 3; r = 0.50) and amount of crystalline Fe (Table 3; r = 0.58) were all positively correlated with P occlusion. In basalt, as weathering and Fe crystallinity increased, P occlusion increased. In andesite, the opposite was true; P occlusion was
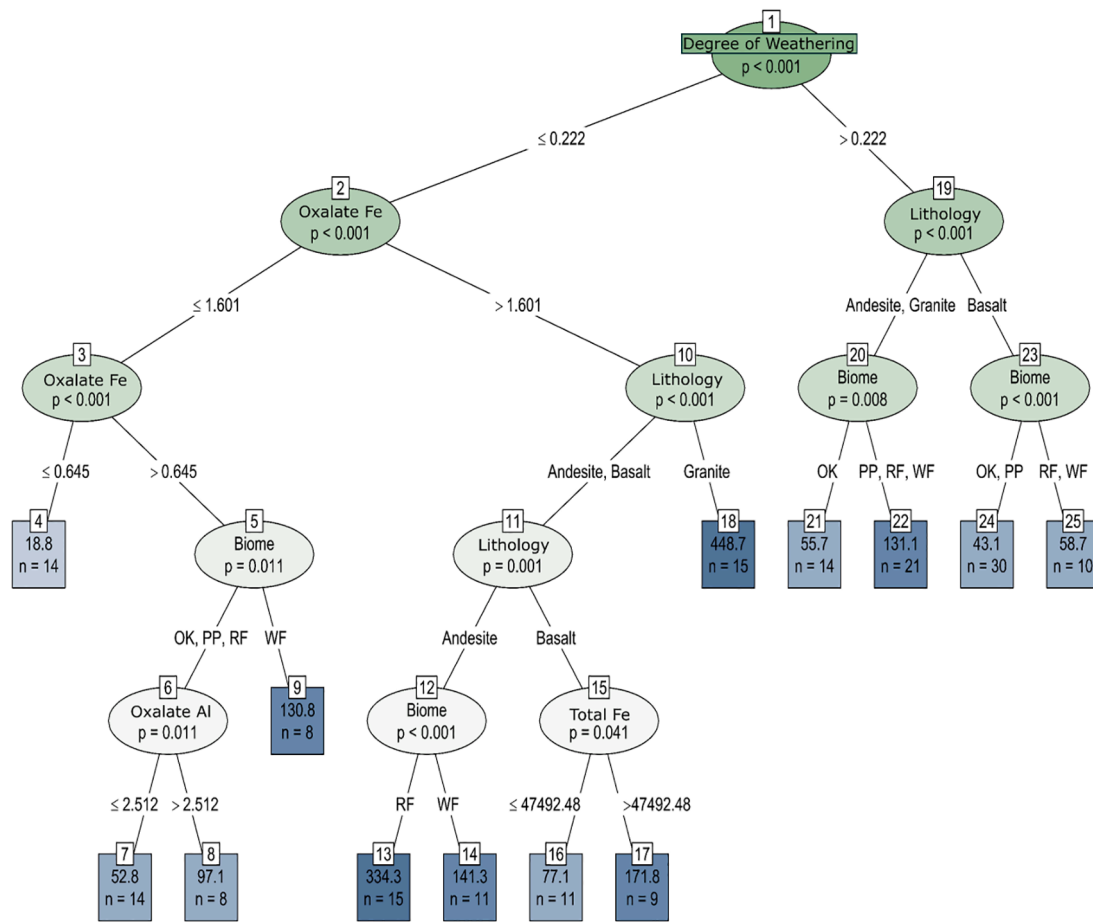
Fig. 6. Conditional inference tree for NaOH-P_i in the solum. P-values indicate a significant relationship between covariate and response in that split of the data. Numbers along branches indicate values of the predictor variable used to make the data split. Numbers in terminal nodes/boxes indicate number of response variable data points (n) and mean of these data points in that partition of the data space.

negatively correlated with the degree of chemical weathering (Table 3; r = −0.55), CIA (Table 3; r = −0.53) and amount of crystalline Fe (Table 3; r = −0.60). In andesite, as weathering and Fe crystallinity increased, P occlusion decreased. In granite, there was a positive relationship between CIA and P occlusion (Table 3; r = 0.33), but not between degree of chemical weathering or Fe crystallinity. Notable among lithologies, a negative relationship existed between Al_o and P occlusion in basalt (Table 3; r = −0.34), and a positive relationship existed between Al_o and P occlusion in andesite (Table 3; r = 0.63).

3.4.6. Total P

In CIT analysis, P_t is primarily associated with poorly crystalline Fe and Al, and secondarily associated with lithology (Fig. 9). The most significant variable splitting P_t was Fe_o concentration, with P_t in soils with high Fe_o best differentiated by Al_o concentrations and parent material. Both samples with high Fe_o and with low Fe_o, were secondarily differentiated by lithology. In nodes defined by lithology, granite and andesite were on one node, and basalt on the other (Fig. 9).

Pedogenic Fe/Al and chemical weathering controls on P_t were evident for andesite and granite, but much less for basalt. In andesite, P_t was retained by poorly crystalline constituents, with significant positive correlations between P_t and Al_o (Table 3; r = 0.74) and Fe_o (Table 3; r = 0.74), and negative correlations with the degree of chemical weathering (Table 3; r = −0.66) and CIA (Table 3; r = -0.70). In granite, P_t was correlated with poorly crystalline constituents, but not measures of chemical weathering (Table 3). In contrast, in basalt P_t was weakly associated with Fe_o (Table 3; r = 0.29, p < 0.05), and not with any

measurement of chemical weathering or Fe/Al-(hydr)oxides.

4. Discussion

The trajectory of soil P dynamics with pedogenesis differs for disparate parent materials experiencing a common climate. Herein, lithology and bioclimatic zone interacted such that the significance of rock type was dissimilar for different fractions and bioclimatic zones. Where a given fraction declined with changes in bioclimate and weathering intensity in one lithology, it increased in another lithology. Thus, pedogenesis is not a march toward a predetermined distribution of P fractions based on time, but instead a complex interaction between climate, biology and lithology dictating the chemical weathering and mineralogical products of pedogenesis.

4.1. Labile P_i

Soils derived from granite generally had higher labile P_i, despite having the lowest rock P content (as much as three-fold lower compared to andesite), consistent with reports from other granitic soils (Adams and Walker, 1975; Claassen and Zasoski, 1998; Tian, 2018; He et al., 2021). Available P has been reported to accumulate via biological nutrient cycling in low P granitic parent materials (He et al., 2021). Soils derived from felsic materials have appreciably lower total Fe and pedogenic Fe oxides compared to basalt and andesite in similar weathering environments (Dahlgren et al., 1997a; Rasmussen et al., 2007; Rasmussen et al., 2010; Wilson et al., 2017). In granite, primary mineral
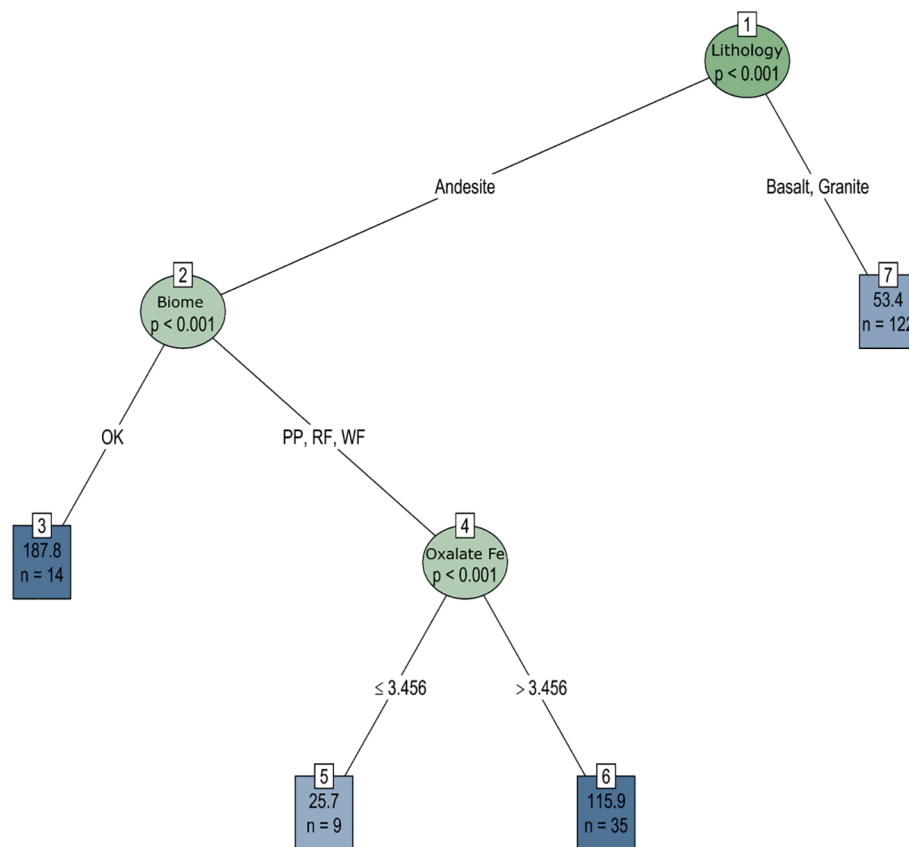
Fig. 7. Conditional inference tree for P_o in the solum. P-values indicate a significant relationship between covariate and response in that split of the data. Numbers along branches indicate values of the predictor variable used to make the data split. Numbers in terminal nodes/boxes indicate number of response variable data points (n) and mean of these data points in that partition of the data space.

Fe for pedogenic Fe-(hydr)oxide generation is lower (*e.g.*, hornblende, biotite in granite vs. pyroxene, olivine in basalt), and the chemical weathering rate and release of Fe is much slower. As such, generation of poorly crystalline aluminosilicates and Fe-(hydr)oxides is much lower, leading to fewer P sorption sites and thereby higher P availability in soils developed from granite.

Andesite-derived soils had the lowest labile P_i, with both the amounts and forms of Fe-(hydr)oxides controlling labile P_i. Poorly crystalline Fe exerts a strong control on P sorption even at low concentrations by virtue of high specific surface area and highly reactive surface groups (Johnson et al., 1986). Moreover, the weakly weathered soils along the andesite transect (RF-4, WF-3) had andic properties (*i.e.*, high allophane/imogolite content) contributing to strong P sorption. In basalt, labile P_i was best explained by measures of chemical weathering. For basalt, as weathering increased, P availability decreased, in agreement with the classical concept of P limitation with increased weathering (Cross and Schlesinger, 1995; Walker and Syers, 1976). In sum, lithology-specific trajectories for labile P_i with weathering occurred across the lithosequences as dictated primarily by the amount and crystallinity of Fe-(hydr)oxides and aluminosilicates.

4.2. HCL-P_i

Changes in HCl-P_i were driven by changes in chemical weathering, with the degree of alteration of primary minerals to secondary minerals differing among lithologies. HCl-P_i declined in basalt and andesite soils while descending the transect, as climatic drivers of weathering increased, but was unchanged in granite due to its greater mineralogical resistance to chemical weathering. The lack of a change in HCl-P_i across

chronosequences has been reported in arid zones due to lower weathering rates (Lajtha and Schlesinger, 1988; Selmants and Hart, 2010) or in chronosequences dominated by pre-weathered parent materials (Izquierdo et al., 2013; Chen et al., 2015). Similar to our findings, no change in HCl-P_i was observed across a granitic elevational transect in China (He et al., 2021). Herein, the lack of change for HCl-P_i in granite descending along the transect can be ascribed to less chemical weathering in coarse grained granite having more resistant minerals (*e.g.*, quartz, K-feldspar), relative to fine grained andesite and basalt with more weatherable primary minerals. Furthermore, granite weathering proceeds by expansion of biotite that favors deep physical weathering of the regolith, relative to more chemically weathering basalt and andesite parent materials (Zhang et al. 2007; Tian et al., 2019). The HCl-P_i fraction in basalt and andesite soils were strongly driven by chemical weathering, and exhibited the asymptotical decline with increased weathering intensity as conceptualized by Walker and Syers (1976). This is in agreement with Crews et al. (1995) report of HCl-P_i depletion after 20,000 years of pedogenesis in basalt, and the low HCl-P_i reported in weathered andesite soils by Dieter et al. (2010). Whereas HCl-P_i was exhausted as a function of time in Walker and Syers (1976) and Crews et al. (1995), our basalt and andesite transects displayed a decline of HCl-P_i driven by differences in bioclimatic zone and changes in chemical weathering.

4.3. NaOH P_i

In both andesite and basalt, NaOH-P_i was negatively associated with both measures of chemical weathering, contrasting with previous work showing increases in NaOH-P_i with increased weathering in Andisols
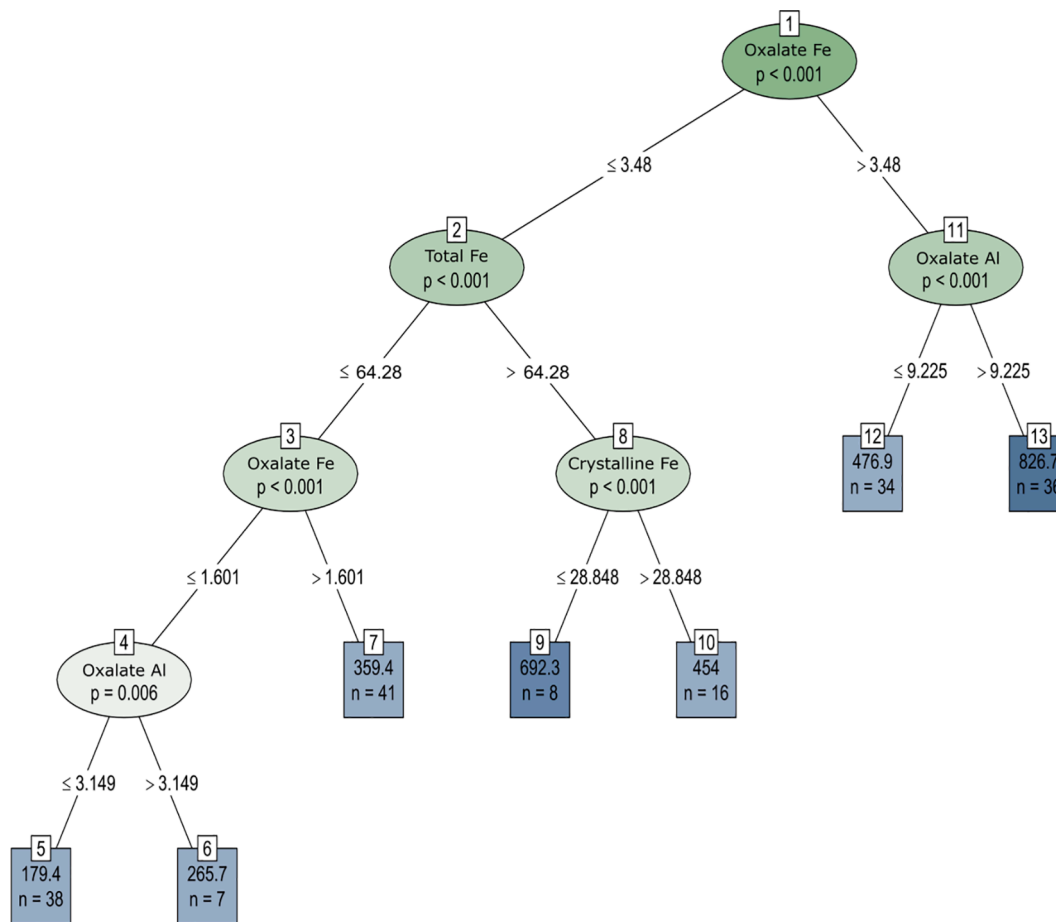
Fig. 8. Conditional inference tree for occluded P in the solum. P-values indicate a significant relationship between covariate and response in that split of the data. Numbers along branches indicate values of the predictor variable used to make the data split. Numbers in terminal nodes/boxes indicate number of response variable data points (n) and mean of these data points in that partition of the data space.

(Cross and Schlesinger, 1995; Satti et al., 2007; Yang and Post, 2011). Mineral crystallinity is favored as the dominant form of precipitation transitions from snow to rain and as temperature increases descending the transects (Dahlgren et al., 1997a; Rasmussen et al., 2007; Rasmussen et al., 2010), thereby contributing to the negative relationship between NaOH-P_i and chemical weathering, and the decline in NaOH-P_i descending the basalt and andesite transects.

4.4. Occluded P

Paradigms of progressive P occlusion with weathering were not uniformly applicable, but rather depended on parent material. Trends and pedogenic controls of occluded P differed by parent material descending the transects. In basalt, increased chemical weathering led to increased P occlusion. However, in andesite occluded P declined with increased weathering, contrasting with Walker and Syers (1976). We interpret this to signify that the contrasting trajectories of P occlusion for each lithology are related to differences in the interaction of weathering and clay mineralogy for the different lithologies, mediated by the amounts and types of clay minerals and Fe/Al-(hydr)oxides. This confirms suspicions by Mage and Porder (2013) that amounts of residual P can be significantly influenced by parent material, and that these differences are attributable to amounts and forms of Fe/Al-oxides. Here, we further the suggestion by Mage and Porder (2013) to include the combined effect of climate and parent material on colloidal constituents (*e.g.* Fe/Al-oxides and aluminosilicates), which in turn influence P occlusion.

In basalt, absolute increases in crystalline Fe-oxide production led to

more P occlusion. This is supported by positive correlations between occluded P, crystalline Fe and measures of chemical weathering. As precipitation decreases and the soil climate becomes drier and warmer with descending elevation, Fe-(hydr)oxides become more crystalline. Since the amount of Fe-(hydr)oxides is a function of rock type in more weathered soils, greater P occlusion occurs in basalt than andesite at more weathered sites. In the basalt transect, P occlusion is driven by extensive weathering of relatively Fe-rich parent materials, leading to larger amounts of crystalline Fe relative to other transects, and increased P occlusion with increased weathering (Crews et al., 1995; Dobermann et al., 2002; Mage and Porder, 2013).

In contrast to basalt, P occlusion in the andesite transect was negatively correlated with measures of chemical weathering and crystalline Fe. As the degree of chemical weathering and crystalline Fe increased, P occlusion decreased. In the andesite transect, the objectively more weathered soil (PP-2), both inferred through soil taxonomy or measures of chemical weathering, had lower P occlusion than less weathered sites (WF-3, RF-4). Correlation analysis suggests that Al_o and Fe_o (andic properties arising from a dominance of ferrihydrite and allophane/imogolite) are the primary drivers of P occlusion in agreement with previous evaluations of Chilean Andisols developed on andesite (Redel et al., 2016). In the andesite transect, P occlusion is driven by transient, poorly crystalline constituents present in the snow-dominated sites that become transformed to crystalline minerals at lower elevations where weathering is more intense. With increased weathering and soil drying, soils transition from having high surface area ferrihydrite and allophane/imogolite to lower surface area, more strongly crystalline Fe/Al-
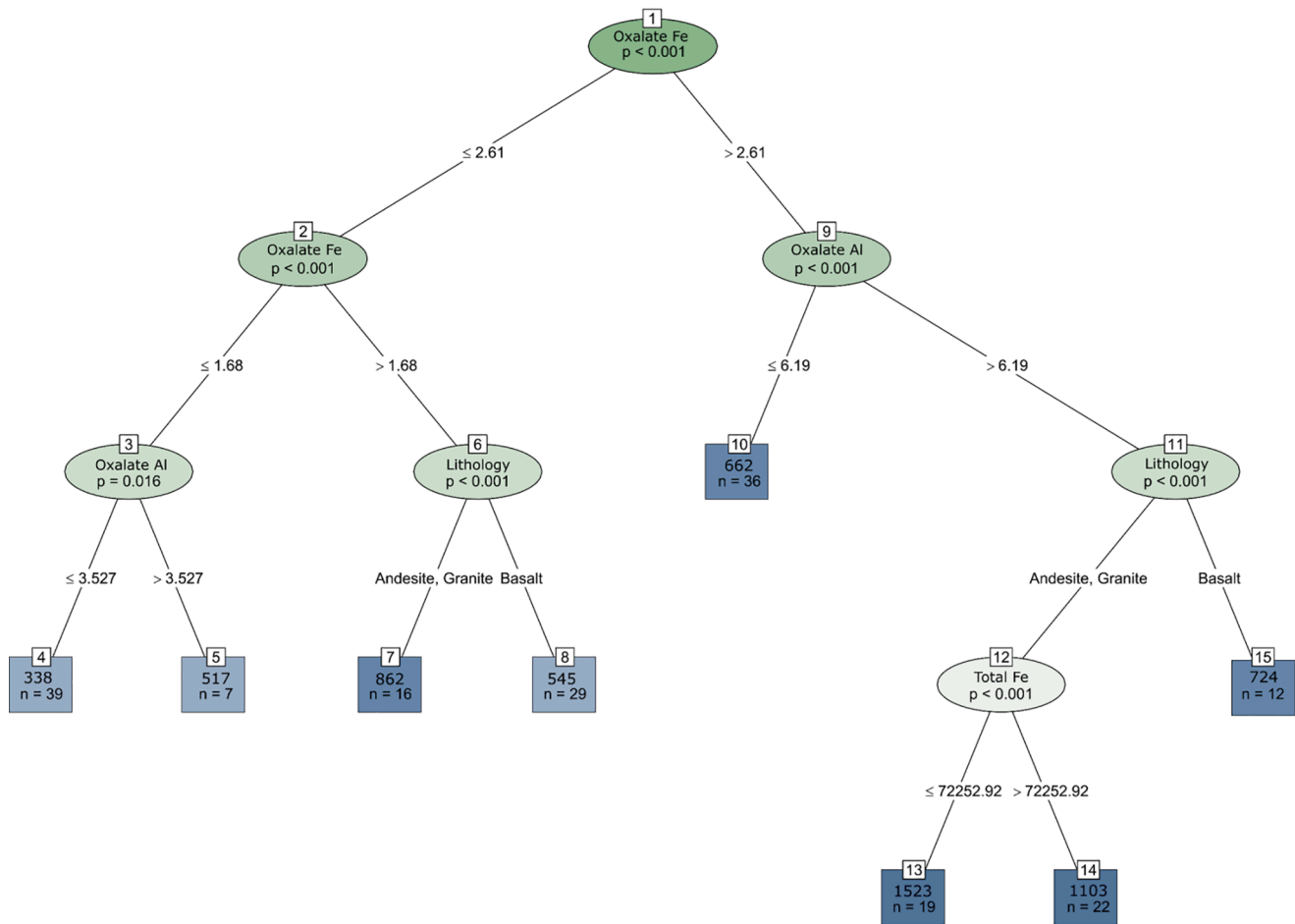
Fig. 9. Conditional inference tree for Total P in the solum. P-values indicate a significant relationship between covariate and response in that split of the data. Numbers along branches indicate values of the predictor variable used to make the data split. Numbers in terminal nodes/boxes indicate number of response variable data points (n) and mean of these data points in that partition of the data space.

(hydr)oxides and kaolin minerals, lessening P occlusion (Parfitt, 1989; Rasmussen et al., 2007). In a chronosequence of Andisols in Mexico, absolute amounts of occluded P declined with increased age, as poorly crystalline materials in younger Andisols shifted to more crystalline minerals in older, more developed soils (Galván-Tejada et al., 2014). These findings are consistent with our findings that changes in P occlusion are driven by changes in soil mineralogy and degree of crystallization of clay minerals.

4.5. Organic P

Soils developed on andesite had overall higher P_o. Lithology, through its influence on P_t, has been reported as a strong driver of P_o (Turner and Engelbrecht, 2011). In higher elevation andesite soils, accumulation of P_o can be explained by higher levels of Al_o and Fe_o and the association of soil organic matter with ferrihydrite, allophane and imogolite (Shoji et al., 1994; Turner et al., 2007; Rasmussen et al., 2018). This was supported by the CIT analysis, where Fe_o was a significant predictor of P_o accumulation in andesite, in agreement with previous work on soil organic C (Rasmussen et al., 2018). Greater amounts of soil organic C have been reported in these andesitic soils, with the largest differences reported at the highest elevation (Rasmussen et al., 2018). While poorly crystalline constituents explain P_o differences in upper elevation sites, the significant lithologic effect on P_o in OK-1 sites is not explained by mineralogy alone. The OK-1 biome showed the greatest differences between lithologies, with more than twice the P_o in andesite than basalt,

and an order of magnitude more P_o compared to granite. P_o trends in OK-1 were similar to trends in lithologic P, with andesite significantly higher than basalt, and basalt significantly higher than granite. Oak-woodland ecosystems concentrate nutrients in surface soils, and litter can be enriched in nutrients when overlying nutrient-rich bedrock, suggesting a potential pathway for P_o enrichment in high P lithologies (Dahlgren et al., 1997b; Morford et al., 2011). Potentially, deep-rooted deciduous trees (*e.g.*, oak) in high P lithologies may accumulate significantly more P in litter inputs, subsequently leading to increased P_o in soils.

4.6. Total P

We suggest differential controls on P_t in soils dependent upon the interaction of state factors, reflected in differences in colloidal constituents and amount, type and degree of weathering. In basalt, P_t does not decline with weathering despite significant alteration of primary minerals (Fe_d/Fe_t) and a strong weathering response (CIA). In basalt, Fe is conserved during pedogenesis and the extensive conversion of primary mineral Fe to pedogenic Fe-oxides leads to the retention of P across chronosequences and weathering gradients in this Fe-rich parent material (Crews et al., 1995; Mage and Porder, 2013; Porder and Ramachandran, 2013). As weathering progresses, Fe-oxides are produced and P is incorporated into the crystalline lattice as occluded P (Mehmood et al., 2018). In the basalt soils reported here and elsewhere, extensive weathering does not lead to a significant decline in

concentrations of P_t (Crews et al., 1995; Porder and Ramachandran, 2013). This is driven both by the accumulation of occluded P in crystalline Fe-oxides, as well as by the maintenance of P_t relative to total mass loss in the weathering of rock to soil (Chadwick et al., 1999). While soil P_t has been reported to decline relative to bedrock P in basalt soils, this was not investigated in the current paper (Chadwick et al., 1999).

In andesite derived soils, P is often retained by poorly crystalline constituents. This is reflected in the very strong positive correlation between P_t and Al_o, and strong negative correlation between P_t and measures of chemical weathering. In andesite, retention of P following release from apatite, is driven by poorly crystalline allophane and imogolite (Parfitt 1989). When P is liberated from glassy apatite it is retained by allophane and imogolite (Brucker and Spohn, 2019; Nanzyo et al., 1997; Nanzyo and Yamasaki, 1998). However, as weathering progresses, poorly crystalline allophane and imogolite transition to kaolin minerals through Ostwald ripening, reducing P retention (Shoji et al. 1994). This leads to significant declines in P_t in andesite with increased chemical weathering.

Soils developed on granite were generally lower in P_t concentrations, reflecting the lower P-content of granite rocks compared to basalt and andesite. However, P_t in granite soils appeared especially enriched compared to granite bedrock. Dust can be a considerable source of P in terrestrial ecosystems, and dust inputs are posited at the granite transect in central California (Chadwick et al., 1999; Aciego et al., 2017). However, should patterns in dust deposition lead to P_t accumulation broadly in these montane ecosystems, a dust induced increase in P_t would be expected across all three transects (Arvin et al. 2017). Yet, the spike in P_t was only observed at mid elevation (WF-3, PP-2) granite sites suggesting that soil enrichment relative to granite rock may not be due to dust deposition, or that dust deposition may be locally specific to granite sites (*e.g.*, locally sourced dust) and not regionally applicable (*e.g.*, globally sourced dust). Alternatively, biological P redistribution can be a significant driver of the disconnect between P_t and rock P (Porder and Chadwick, 2009). Furthermore, it was recently reported that deeply rooted trees overlying deep regolith might preferentially extract available P (Hauser et al. 2021). Given the deep physical weathering of granite (as much as 10 m) at mid elevation sites (WF-3, PP-2) and significant P availability in this deep regolith, it is conceivable that higher levels of P_t, as well as labile P_i, in the granitic solum are the result of biological pumping of P by deep rooted conifers, enriching soil P relative to rock (Hubbert et al., 2001; Graham et al., 2010; Porder and Chadwick, 2009; Hahm et al., 2014; Tian, 2018; Tian et al., 2019; Hauser et al., 2021; He et al., 2021). Thus, deep physical weathering of granite having a low inherent P content magnifies the differences between rock P and soil P, as trees extract P from regolith and cycle it back to the soil surface (Porder and Chadwick, 2009; He et al., 2021). However, more research is needed to disentangle dust versus biological P pumping mechanisms leading to elevated soil P at granite sites.

5. Conclusion: Expanding the paradigm

We demonstrate that lithology and climate interact to influence the distribution of soil P more profoundly than previously reported in chronosequence studies. Lithology informed both the relative magnitude of P fractions and how these fractions respond to pedogenic transformations governed by climate. Differences in the interaction of climate and lithology led to differences in the amount and composition of the clay fraction, which in turn affected differences in mechanisms that regulate P dynamics. In partial confirmation of our hypothesis, the

amounts and crystallinity of Fe-(hydr)oxides significantly influenced P dynamics. We postulated that higher Fe content in soils from more mafic parent materials would lead to more occluded P and less labile P_i. However, the relationship between P fractions and lithology was found to be more complex, involving degree of crystallinity of Fe/Al-(hydr) oxides, abundance of poorly crystalline aluminosilicates (allophane, imogolite), and degree of chemical weathering. In contrast to concepts of P limitation inherent in low P lithologies, granite soils were uniformly highest in labile P_i whereas soils developed on high P andesite were uniformly lower in labile P_i. This reflects slower weathering rates and lower production of Fe-(hydr)oxides in granite parent materials, and more poorly crystalline constituents in andesitic soils that strongly fix P. Therefore, the ecological availability of P is tied to pedogenic state factors as integrated through mineralogy. Basalt soils, showing evidence of more intense chemical weathering, exhibited the Walker-Syers model asymptotical decline in HCl-P_i, while granite, with less chemical weathering, was relatively unchanged. Occluded P provided the best example of the differential effects of the bioclimatic gradient on disparate parent materials. In andesite, occluded P decreased with increased weathering, a trend opposite that in basalt and the Walker and Syers model. In granite, occluded P was constant across the bioclimatic gradient. In andesite, P occlusion was driven more by the degree of crystallinity of Fe-(hydr)oxides and aluminosilicates than the degree of weathering, contrasting with established concepts of increased P occlusion with increased weathering. Lithology was a strong driver of P_o, with andesite broadly higher in P_o, especially in the OK-1 biome. Significant lithologic differences in soil P_o in OK-1 may reflect magnification of lithologic P differences due to accumulation of P_o in deciduous oak woodlands. In basalt, concentrations of P_t are maintained by crystalline Fe-oxides as weathering progresses since crystalline Fe-oxides increase with increased weathering. In andesite, P_t retention is tied to liberation from apatite and subsequent binding to allophane and imogolite. As these minerals transition to kaolinite with increased weathering, P retention capacity decreases resulting in declining P_t. In granite, deep physical weathering, biological P redistribution and potentially regional dust inputs, lead to pronounced differences between lithologic P and soil P_t.

Our results demonstrate that lithology, as a key pedogenic state factor, influences the fate of P during pedogenesis more broadly than previously recognized, not just influencing the absolute amount of P, but also contributing to a complex set of relationships integrating soil mineralogy, chemical and physical weathering and bioclimatic zone. Soils from disparate lithologies experiencing a similar climate have different pedogenic trajectories, and subtle-to-substantial differences in weathering products, leading to broadly different P dynamics. This work informs future efforts concerning biogeochemical P cycling by revealing that the fate of P in response to pedogenic transformations involves nuanced interactions among pedogenic state factors.

Declaration of Competing Interest

The authors declare that they have no known competing financial interests or personal relationships that could have appeared to influence the work reported in this paper.

Acknowledgements

Appendix A

Hedley phosphorus fractions for each combination of bioclimatic zone and bedrock lithology for representative pedons and horizons.

Biome	PM	Depth	Resin Pi	NaHCO$_3$ Pi	Labile[1] Pi	NaCO$_3$ Po	NaOH Pi	NaOH Po	Ca Pi	Organic[2] P	Total[3] P	Occluded[4] P
		cm	mg kg^{-1}									
Red fir	Basalt	3–8	16.57	4.96	21.5	22.7	81.2	28.8	119.1	51.5	611.0	337.6
		8–15	3.31	5.64	8.9	1.7	85.4	15.6	161.2	17.2	480.0	207.3
		15–30	1.82	<0.01	1.8	5.5	158.9	40.3	148.8	45.8	654.6	299.3
		30–48	1.63	<0.01	1.6	4.5	146.7	27.1	141.1	31.6	611.0	289.9
		48–76	1.10	<0.01	1.1	2.5	99.4	26.1	60.4	28.6	480.0	290.6
White fir	Basalt	0–10	8.05	4.93	13.0	37.1	97.1	97.2	161.7	134.2	916.4	510.4
		10–19	1.63	<0.01	1.6	6.6	74.1	47.7	37.5	54.4	523.7	356.1
		19–40	1.77	<0.01	1.8	4.2	50.0	35.1	26.9	39.3	436.4	318.4
		40–60	1.09	<0.01	1.1	3.2	43.0	26.4	38.4	29.6	436.4	324.3
		60–100	0.61	0.10	0.7	2.3	41.1	11.0	33.3	13.2	392.8	304.4
Ponderosa pine	Basalt	0–7	9.96	0.67	10.6	23.8	60.1	108.5	7.7	132.4	785.5	574.7
		7–18	3.84	0.21	4.1	19.6	56.3	80.7	2.8	100.3	654.6	491.1
		18–28	0.61	<0.01	0.6	11.3	51.0	73.5	0.8	84.8	611.0	473.8
		28–49	0.60	<0.01	0.6	5.7	41.2	49.1	<0.1	54.9	523.7	427.0
		49–75	0.25	1.96	2.2	3.4	29.4	27.3	<0.1	30.7	392.8	330.4
Oak	Basalt	0–5	3.53	1.70	5.2	17.5	45.9	88.9	16.4	106.3	741.9	568.0
		5–16	1.68	2.16	3.8	6.2	54.2	38.3	14.8	44.5	654.6	537.3
		16–27	2.57	1.96	4.5	5.8	49.8	39.1	7.9	44.9	654.6	547.4
		27–44	2.81	0.21	3.0	5.3	43.1	28.5	4.1	33.8	611.0	526.9
		44–50	1.57	1.59	3.2	4.4	13.0	17.2	1.1	21.6	436.4	397.5
Red fir	Andesite	0–7	0.01	1.06	1.1	1.7	482.8	44.3	29.8	46.0	1571.0	1011.4
		7–25	<0.01	0.26	0.3	1.1	336.7	108.8	25.1	109.9	1352.8	880.9
		25–43	0.03	0.14	0.2	0.7	285.6	96.2	17.7	96.9	1091.0	690.6
		43–63	<0.01	0.10	0.1	0.7	236.1	162.6	14.5	163.2	960.1	546.1
		63–85	<0.01	0.13	0.1	0.7	247.0	131.2	11.6	131.9	872.8	482.2
White fir	Andesite	0–16	0.29	0.54	0.8	1.7	90.4	160.7	34.0	162.4	1571.0	1283.4
		16–32	<0.01	0.23	0.2	1.2	111.9	154.4	25.0	155.7	1396.5	1103.7
		32–53	<0.01	0.14	0.1	0.8	130.9	137.7	17.6	138.5	1178.3	891.1
		53–85	<0.01	0.17	0.2	0.6	197.5	105.8	15.1	106.4	1178.3	859.1
Ponderosa pine	Andesite	0–10	0.62	0.70	1.3	2.5	182.8	185.4	6.9	187.9	1440.1	1061.2
		10–40	0.04	0.18	0.2	0.7	191.5	167.0	1.9	167.7	1178.3	817.0
		40–60	<0.01	0.21	0.2	0.5	193.7	154.3	1.4	154.8	1091.0	740.9
		60–100	0.63	0.09	0.7	0.2	94.8	114.8	0.3	115.0	611.0	400.2
		100–158	<0.01	0.12	0.1	0.1	99.8	89.0	0.3	89.1	611.0	421.6
		158–200	<0.01	0.25	0.2	0.1	90.9	60.9	0.4	60.9	654.6	502.1
Oak	Andesite	0–12	0.58	0.27	0.8	1.8	72.9	224.5	3.1	226.3	829.2	526.0
		12–29	0.31	0.32	0.6	1.1	82.3	220.9	3.0	222.1	872.8	564.8
		29–45	0.13	0.26	0.4	0.7	56.4	206.8	1.7	207.5	654.6	388.6
		45–65	0.01	0.17	0.2	0.6	41.6	174.9	0.8	175.5	523.7	305.6
		65–90	0.07	0.14	0.2	0.3	53.2	125.2	0.6	125.4	480.0	300.6
Red fir	Granite	0–7	23.36	9.39	32.7	92.8	63.0	110.0	47.2	202.9	611.0	265.2
		7–21	1.54	9.07	10.6	15.9	113.4	43.8	38.0	59.7	392.8	171.1
		21–42	0.43	5.40	5.8	12.3	97.3	48.6	33.2	60.9	349.1	152.0
		42–94	0.04	7.08	7.1	8.4	112.4	42.4	40.0	50.7	349.1	138.9
		94–121	0.87	6.67	7.5	11.0	110.3	48.6	26.1	59.5	349.1	145.6
		121–140	0.23	4.68	4.9	6.3	52.9	16.8	7.6	23.1	218.2	129.6
White fir	Granite	0–6	32.73	34.79	67.5	41.0	229.9	66.3	129.0	107.2	872.8	339.1
		6–15	22.44	36.12	58.6	28.9	270.0	31.0	107.3	59.9	872.8	377.2
		15–36	2.81	6.17	9.0	5.6	134.1	31.5	61.9	37.0	480.0	238.0
		36–70	3.36	5.77	9.1	4.4	115.7	24.6	49.2	29.0	436.4	233.3
		70–95	2.47	3.48	5.9	3.3	62.4	17.0	29.9	20.3	261.8	143.3
		95–151	2.47	3.30	5.8	2.4	40.1	13.6	30.2	16.0	218.2	126.2
Ponderosa pine	Granite	0–9	41.13	49.42	90.6	23.9	432.2	58.2	184.2	82.1	1091.0	302.0
		9–30	36.60	55.72	92.3	21.7	492.9	57.1	144.7	78.8	1091.0	282.3
		30–46	24.38	19.08	43.5	9.6	266.6	64.0	102.0	73.5	741.9	256.3
		46–70	9.14	7.08	16.2	6.6	83.0	36.3	47.4	42.9	392.8	203.3
		70–102	4.34	6.05	10.4	4.1	39.0	14.3	29.1	18.4	261.8	164.9
		102–160	3.51	8.27	11.8	5.5	49.3	6.6	25.1	12.0	261.8	163.7
		160–200	5.41	8.73	14.1	6.4	60.5	22.2	38.2	28.6	305.5	164.1
Oak	Granite	0–10	27.18	9.87	37.0	8.9	22.2	31.6	175.1	40.5	480.0	205.2
		10–37	31.15	9.01	40.2	3.1	21.7	17.6	219.6	20.7	480.0	178.0
		37–78	27.83	8.38	36.2	1.2	17.8	13.7	157.1	15.0	392.8	166.7
		78–112	11.46	4.87	16.3	1.1	12.5	5.0	58.6	6.1	261.8	168.3

[1]Sum of resin Pi and NaHCO$_3$ Pi. [2]Sum of NaHCO$_3$ and NaOH P$_o$ fractions. [3]Total P from lithium borate fusion. [4]Difference between total P and sum of Hedley P fractions.

Appendix B

Selective dissolution, measures of chemical weathering and total Fe for representative pedons and horizons for each combination of bioclimatic zone and lithology.

Biome	PM	Depth	Al_o[1]	Fe_o[2]	Fe_d[3]	Fe_d-Fe_o[4]	CIA[5]	Fe_d/Fe_t[6]	Fe_t[7]
		cm	_____ $g\ kg^{-1}$ _____				___ratio___		$g\ kg^{-1}$
Red fir	Basalt	3–8	2.9	2.7	3.2	0.5	47.5	0.1	38.6
		8–15	5.1	2.6	3.9	1.3	50.6	0.1	36.9
		15–30	14.6	3.2	9.2	6.0	58.0	0.1	63.3
		30–48	17.6	3.5	8.9	5.4	59.0	0.1	63.4
		48–76	15.3	3.1	8.8	5.7	58.8	0.1	64.3
White fir	Basalt	0–10	18.1	2.5	6.6	4.1	57.8	0.2	38.3
		10–19	23.2	2.4	9.2	6.8	60.5	0.2	45.3
		19–40	23.4	2.1	11.5	9.5	62.5	0.2	48.8
		40–60	24.2	2.5	12.0	9.4	63.6	0.2	50.6
		60–100	29.8	2.3	16.0	13.7	65.9	0.3	56.5
Ponderosa pine	Basalt	0–7	8.3	2.5	48.3	45.8	90.6	0.6	83.2
		7–18	8.7	2.3	51.3	49.0	93.1	0.6	89.1
		18–28	8.0	2.1	54.4	52.3	94.4	0.6	93.5
		28–49	5.5	2.0	58.5	56.5	95.6	0.6	95.3
		49–75	3.6	1.7	59.6	57.9	97.8	0.7	90.8
Oak	Basalt	0–5	2.0	7.5	56.1	48.6	85.5	0.6	101.8
		5–16	1.8	4.1	55.9	51.8	88.1	0.5	104.6
		16–27	1.9	4.3	55.0	50.8	88.3	0.5	105.3
		27–44	1.9	4.5	53.1	48.6	89.1	0.5	102.8
		44–50	1.9	4.6	42.5	37.9	89.1	0.4	95.3
Red fir	Andesite	0–7	26.7	5.2	8.8	3.6	70.6	0.1	71.8
		7–25	34.7	5.9	11.3	5.4	72.6	0.2	71.8
		25–43	33.7	6.0	11.5	5.5	72.9	0.2	73.4
		43–63	32.1	6.0	11.3	5.3	73.1	0.2	73.4
		63–85	27.7	5.4	9.5	4.1	72.1	0.1	75.7
White fir	Andesite	0–16	31.1	6.4	12.3	5.9	67.4	0.2	56.2
		16–32	38.5	7.7	15.6	7.9	72.4	0.2	69.6
		32–53	39.9	7.7	16.8	9.1	72.0	0.2	77.4
		53–85	34.9	6.7	15.2	8.5	71.3	0.2	81.1
Ponderosa pine	Andesite	0–10	13.5	4.1	38.9	34.8	91.3	0.5	72.3
		10–40	16.0	4.6	44.8	40.2	96.1	0.5	88.1
		40–60	15.5	4.7	46.7	42.0	96.8	0.5	91.0
		60–100	8.3	4.4	48.5	44.1	97.5	0.5	90.9
		100–158	4.1	4.9	49.0	44.1	98.1	0.5	90.4
		158–200	3.6	3.6	42.9	39.3	98.4	0.5	90.5
Oak	Andesite	0–12	4.0	4.0	32.0	28.0	89.6	0.4	77.9
		12–29	4.1	4.2	35.8	31.6	90.9	0.4	82.1
		29–45	3.4	4.5	38.0	33.4	92.0	0.5	82.5
		45–65	2.9	4.7	39.8	35.1	93.8	0.5	82.1
		65–90	2.8	4.8	40.7	35.9	95.8	0.5	80.2
Red fir	Granite	0–7	3.1	1.1	2.2	1.1	58.6	0.1	15.6
		7–21	2.7	1.1	2.4	1.4	59.1	0.1	16.5
		21–42	3.5	1.4	2.8	1.4	59.6	0.2	17.1
		42–94	2.8	1.0	2.2	1.3	58.5	0.1	15.9
		94–121	3.1	1.5	2.6	1.1	58.8	0.1	17.6
		121–140	1.1	1.3	3.1	1.9	62.3	0.2	13.8
White fir	Granite	0–6	4.8	1.5	2.6	1.1	57.6	0.1	26.3
		6–15	6.7	1.7	2.5	0.8	58.5	0.1	29.0
		15–36	5.1	1.6	2.2	0.6	59.7	0.1	31.8
		36–70	4.0	1.4	2.5	1.1	60.6	0.1	34.9
		70–95	2.1	0.9	2.3	1.3	62.0	0.1	35.3
		95–151	1.5	0.6	1.8	1.1	61.8	0.1	32.9
Ponderosa pine	Granite	0–9	4.2	1.7	3.3	1.6	60.6	0.1	36.2
		9–30	4.2	1.9	3.4	1.5	61.6	0.1	38.3
		30–46	3.0	1.9	4.0	2.2	63.3	0.1	40.8
		46–70	1.2	1.1	4.0	3.0	63.5	0.1	41.8
		70–102	0.7	0.8	3.9	3.1	64.4	0.1	40.1
		102–160	1.1	0.8	4.4	3.6	68.0	0.1	37.7
		160–200	1.1	0.8	3.4	2.6	64.3	0.1	36.7
Oak	Granite	0–10	0.4	0.6	1.5	1.2	54.2	0.1	26.4
		10–37	0.4	0.5	1.7	1.3	54.1	0.1	25.3
		37–78	0.3	0.6	1.8	1.3	54.3	0.1	29.4
		78–112	0.3	0.5	1.9	1.7	54.8	0.1	35.5

[1]Oxalate Extractable Al. [2]Oxalate extractable Fe. [3]Dithionite extractable Fe. [4]Crystalline Fe (hydr)oxides (Fe_d-Fe_o). [5]Chemical Index of Alteration: $[Al_2O_3/(Al_2O_3 + Na_2O + CaO + K_2O)] \times 100$ [6] Degree of weathering, the ratio of pedogenic Fe (Fe_d) to total Fe. [7]Total Fe from lithium borate fusion.

Appendix C

Major oxides for select pedons and horizons for each combination of bioclimatic zone and lithology. Total elemental analysis by lithium borate fusion.

| Biome	PM	Depth	Horizon	Al_2O_3	Fe_2O_3	K_2O	MgO	Na_2O	P_2O_5	SiO_2	CaO
		cm	Wt%								
Red fir	Basalt	3–8	A	15.31	5.52	1.56	4.07	3.24	0.14	55.34	5.44
		8–15	C	16.30	5.27	1.63	3.47	3.48	0.11	59.44	4.65
		15–30	2Ab	18.09	9.05	0.86	6.50	2.32	0.15	50.17	4.60
		30–48	2Bwb1	18.53	9.06	0.82	6.55	2.28	0.14	49.72	4.52
		48–76	2Bwb2	18.57	9.19	0.76	7.06	2.32	0.11	50.45	4.60
White fir	Basalt	0–10	A	16.69	5.48	1.25	2.66	2.39	0.21	44.16	3.80
		10–19	AB	19.80	6.48	1.37	3.26	2.80	0.12	51.68	3.76
		19–40	BW1	20.92	6.98	1.26	3.40	2.71	0.10	51.35	3.71
		40–60	Bw2	21.42	7.23	1.13	3.72	2.59	0.10	50.17	3.74
		60–100	BC	22.2	8.08	0.85	5.32	2.08	0.09	47.50	3.93
Ponderosa pine	Basalt	0–7	A	24.58	11.90	0.42	0.74	0.30	0.18	35.35	0.88
		7–18	AB	26.56	12.74	0.42	0.72	0.31	0.15	37.76	0.56
		18–28	Bt1	27.51	13.37	0.40	0.73	0.30	0.14	39.58	0.38
		28–49	Bt2	28.35	13.62	0.36	0.60	0.22	0.12	40.29	0.30
		49–75	Bt3	30.35	12.98	0.20	0.30	0.08	0.09	38.67	0.19
Oak	Basalt	0–5	A	20.68	14.56	0.42	1.19	0.66	0.17	46.43	1.08
		5–16	Bt1	21.72	14.96	0.41	1.14	0.60	0.15	46.76	0.82
		16–27	Bt2	22.01	15.06	0.41	1.18	0.59	0.15	46.80	0.83
		27–44	Bt3	22.11	14.70	0.39	1.00	0.57	0.14	46.92	0.74
		44–50	Bt4	22.37	13.62	0.31	1.17	0.56	0.10	47.48	0.82
Red fir	Andesite	0–7	A1	21.36	10.26	0.76	4.03	1.44	0.36	39.56	3.14
		7–25	A2	22.64	10.26	0.72	3.92	1.45	0.31	40.30	2.96
		25–43	Bw1	22.99	10.50	0.72	4.05	1.47	0.25	41.44	2.95
		43–63	Bw2	22.96	10.49	0.67	4.06	1.43	0.22	41.58	2.96
		63–85	BC	23.06	10.82	0.60	4.34	1.46	0.20	42.37	3.23
White fir	Andesite	0–16	A1	17.00	8.04	0.72	2.63	0.99	0.36	30.94	3.19
		16–32	A2	21.09	9.95	0.81	3.20	1.20	0.32	36.97	2.86
		32–53	Bw1	21.90	11.06	0.84	3.79	1.27	0.27	40.13	3.03
		53–85	Bw2	21.78	11.59	0.86	4.08	1.29	0.27	41.31	3.15
Ponderosa pine	Andesite	0–10	A	24.50	10.33	0.34	0.39	0.11	0.33	30.06	0.98
		10–40	ABt	29.96	12.60	0.37	0.40	0.12	0.27	35.28	0.34
		40–60	Bt1	30.67	13.01	0.38	0.39	0.11	0.25	36.52	0.24
		60–100	Bt2	31.24	12.99	0.40	0.33	0.05	0.14	37.09	0.15
		100–158	Bt3	31.07	12.92	0.33	0.30	0.03	0.14	38.07	0.11
		158–200	Bt4	30.73	12.94	0.26	0.28	0.03	0.15	39.60	0.09
Oak	Andesite	0–12	A	24.21	11.14	0.93	0.58	0.42	0.19	43.54	0.62
		12–29	ABt	25.64	11.74	0.93	0.55	0.39	0.20	44.38	0.51
		29–45	Bt1	26.24	11.8	0.88	0.49	0.36	0.15	44.78	0.41
		45–65	Bt2	27.48	11.74	0.69	0.43	0.28	0.12	44.29	0.33
		65–90	Bt3	28.53	11.46	0.47	0.39	0.18	0.11	43.34	0.25
Red fir	Granite	0–7	A	12.17	2.23	3.49	0.41	1.82	0.14	58.15	1.00
		7–21	AB	14.24	2.36	4.26	0.40	2.08	0.09	70.38	1.01
		21–42	Bw1	14.64	2.45	4.17	0.45	2.15	0.08	68.94	1.02
		42–94	Bw2	14.92	2.28	4.38	0.41	2.34	0.08	70.12	1.10
		94–121	BC	14.82	2.52	4.40	0.42	2.24	0.08	69.46	1.06
		121–140	Cr	14.34	1.98	4.51	0.27	1.56	0.05	72.32	0.67
White fir	Granite	0–6	A1	14.38	3.76	3.00	1.28	1.95	0.2	55.16	2.28
		6–15	A2	15.90	4.15	3.20	1.4	2.16	0.2	58.65	2.35
		15–36	AB	17.11	4.54	3.30	1.54	2.16	0.11	63.57	2.44
		36–70	Bw1	17.44	4.99	3.08	1.72	2.04	0.1	62.01	2.55
		70–95	Bw2	17.46	5.04	2.98	1.76	1.87	0.06	62.32	2.43
		95–151	BC	17.08	4.71	3.06	1.66	1.92	0.05	63.58	2.49
Ponderosa pine	Granite	0–9	A1	16.01	5.17	2.00	1.72	1.91	0.25	60.13	2.81
		9–30	A2	17.12	5.48	2.06	1.82	2.03	0.25	61.63	2.81
		30–46	AB	18.50	5.83	2.08	1.96	2.01	0.17	61.15	2.85
		46–70	Bw	18.34	5.97	2.10	2.03	1.94	0.09	61.04	2.8
		70–102	Bt1	17.00	5.73	1.90	2.00	1.70	0.06	63.7	2.49
		102–160	Bt2	20.69	5.39	1.47	1.78	1.88	0.06	58.1	2.78
		160–200	Cr	18.91	5.25	1.81	1.80	2.03	0.07	60.31	2.87
Oak	Granite	0–10	A	15.37	3.78	1.75	1.35	3.09	0.11	65.23	3.32
		10–37	AB	15.50	3.62	1.71	1.29	3.17	0.11	67.77	3.34
		37–78	Bt1	15.98	4.20	1.68	1.52	3.15	0.09	66.43	3.55
		78–112	Bt2	17.36	5.07	1.71	2.06	3.15	0.06	62.97	4.01

Appendix D
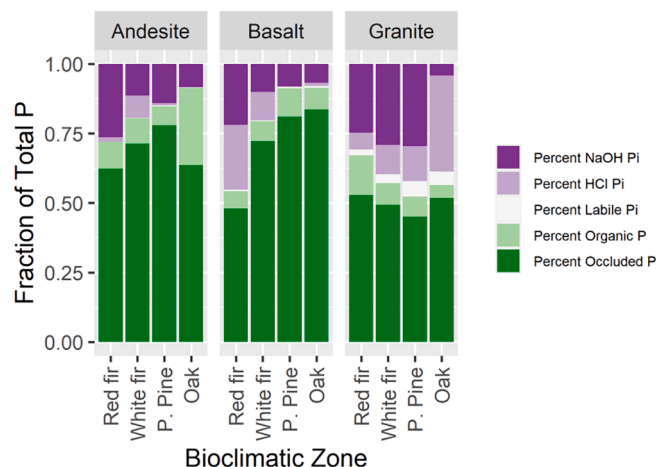
Fig. 10. Depth weighted mean in solum proportion of P in fractions relative to total P for each lithology. Data show the effect of bioclimate and weathering gradient for each rock type.
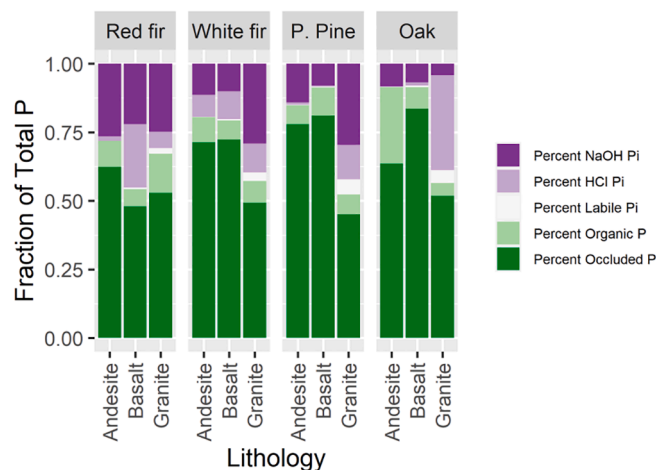

Fig. 11. Depth weighted mean in solum proportion of P in fractions relative to total P for each lithology. Data show the effect of lithology within each bioclimatic zone.

References

Aciego, S.M., Riebe, C., Hart, S., Blakowski, M., Carey, C., Aarons, S., Dove, N., Botthoff, J., Sims, K., Aronson, E., 2017. Dust outpaces bedrock in nutrient supply to montane forest ecosystems. Nat. Commun. 8, 1–10.

Adams, J., Walker, T., 1975. Some properties of a chrono-toposequence of soils from granite in New Zealand, 2. Forms and amounts of phosphorus. *Geoderma* 13, 41–51.

Alexander, E.B., Mallory, J.I., Colwell, W.L. (1993). Soil-elevation relationships on a volcanic plateau in the southern Cascade Range, northern California, USA. *Catena, 20*(1-2), 113-128.

Arvin, L.J., Riebe, C.S., Aciego, S.M., Blakowski, M.A., 2017. Global patterns of dust and bedrock nutrient supply to montane ecosystems. Sci. Adv. 3 (12), eaao1588.

Augusto, L., Achat, D.L., Jonard, M., Vidal, D., Ringeval, B., 2017. Soil parent material—A major driver of plant nutrient limitations in terrestrial ecosystems. Glob. Change Biol. 23 (9), 3808–3824.

Barrow, N.J., Sen, A., Roy, N., Debnath, A., 2021. The soil phosphate fractionation fallacy. Plant Soil 459, 1–11.

Burt, R., Staff, S., 2014. Kellogg Soil Survey Laboratory Methods Manual. Natural Resources Conservation Services. National Soil Survey Center, Lincoln, Nebraska.

Brucker, E., Spohn, M., 2019. Formation of soil phosphorus fractions along a climate and vegetation gradient in the Coastal Cordillera of Chile. Catena 180, 203–211.

Buol, S.W., Southard, R.J., Graham, R.C., McDaniel, P.A., 2011. Soil Genesis and Classification. John Wiley & Sons.

Chadwick, O.A., Derry, L.A., Vitousek, P.M., Huebert, B.J., Hedin, L.O., 1999. Changing sources of nutrients during four million years of ecosystem development. Nature 397, 491–497.

Chen, C.R., Hou, E.Q., Condron, L.M., Bacon, G., Esfandbod, M., Olley, J., Turner, B.L., 2015. Soil phosphorus fractionation and nutrient dynamics along the Cooloola coastal dune chronosequence, southern Queensland, Australia. Geoderma 257, 4–13.

Claassen, V., Zasoski, R., 1998. A comparison of plant available nutrients on decomposed granite cut slopes and adjacent natural soils. Land Degrad. Dev. 9, 35–46.

Crews, T.E., Kitayama, K., Fownes, J.H., Riley, R.H., Herbert, D.A., Mueller-Dombois, D., Vitousek, P.M., 1995. Changes in soil phosphorus fractions and ecosystem dynamics across a long chronosequence in Hawaii. Ecology 76, 1407–1424.

Cross, A.F., Schlesinger, W.H., 1995. A literature review and evaluation of the. Hedley fractionation: applications to the biogeochemical cycle of soil phosphorus in natural ecosystems. Geoderma 64, 197–214.

Dahlgren, R., Boettinger, J., Huntington, G., Amundson, R., 1997a. Soil development along an elevational transect in the western Sierra Nevada, California. Geoderma 78, 207–236.

Dahlgren, R.A., Singer, M.J., Huang, X., 1997b. Oak tree and grazing impacts on soil properties and nutrients in a California oak woodland. Biogeochemistry 39, 45–64.

Delgado-Baquerizo, M., Reich, P.B., Bardgett, R.D., Eldridge, D.J., Lambers, H., Wardle, D.A., Fierer, N., 2020. The influence of soil age on ecosystem structure and function across biomes. Nat. Commun. 11 (1), 1–14.

Dieter, D., Elsenbeer, H., Turner, B.L., 2010. Phosphorus fractionation in lowland tropical rainforest soils in central Panama. Catena 82, 118–125.

Dobermann, A., George, T., Thevs, N., 2002. Phosphorus fertilizer effects on soil phosphorus pools in acid upland soils. Soil Sci. Soc. Am. J. 66 (2), 652–660.

Ducea, M., 2001. The California arc: thick granitic batholiths, eclogitic residues, lithospheric-scale thrusting, and magmatic flare-ups. GSA Today 11 (11), 4–10.

Frost, B.R., Barnes, C.G., Collins, W.J., Arculus, R.J., Ellis, D.J., Frost, C.D., 2001. A geochemical classification for granitic rocks. J. Petrol. 42 (11), 2033–2048.

Galván-Tejada, N.C., Peña-Ramírez, V., Mora-Palomino, L., Siebe, C., 2014. Soil P fractions in a volcanic soil chronosequence of Central Mexico and their relationship to foliar P in pine trees. J. Plant Nutr. Soil Sci. 177, 792–802.

Gillespie, A.R., & Zehfuss, P.H. (2004). Glaciations of the sierra Nevada, California, USA. In Developments in quaternary sciences (Vol. 2, pp. 51-62). Elsevier.

Graham, R.C., Rossi, A.M., Hubbert, R., 2010. Rock to regolith conversion: Producing hospitable substrates for terrestrial ecosystems. GSA Today 20, 4–9.

Griffith, G.E., Omernik, J.M., Smith, D.W., Cook, T.D., Tallyn, E.D., Moseley, K., Johnson, C.B. (2016). Ecoregions of California. US Geological Survey Open-File Report, 1021.

Gu, C., Wilson, S.G., Margenot, A.J., 2020a. Lithological and bioclimatic impacts on soil phosphatase activities in California temperate forests. Soil Biol. Biochem. 141, 107633.

Gu, C., Dam, T., Hart, S.C., Turner, B.L., Chadwick, O.A., Berhe, A.A., Hu, Y., Zhu, M., 2020b. Quantifying uncertainties in sequential chemical extraction of soil phosphorus using XANES spectroscopy. Environ. Sci. Technol. 54, 2257–2267.

Gu, C., Margenot, A.J., 2021. Navigating limitations and opportunities of soil phosphorus fractionation. Plant Soil 459, 13–17.

Hahm, W.J., Riebe, C.S., Lukens, C.E., Araki, S., 2014. Bedrock composition regulates mountain ecosystems and landscape evolution. Proc. Natl. Acad. Sci. 111, 3338–3343.

Hauser, E., Chorover, J., Cook, C., Markewitz, D., Rasmussen, C., Richter, D., Billings, S. Walker and Syers enter the critical zone: Integrating decadal scale root development with longer term soil development to understand terrestrial nutrient cycling. *Authorea* 2021 (in review).

He, X., Chu, C., Yang, Y., Shu, Z., Li, B., Hou, E., 2021. Bedrock and climate jointly control the phosphorus status of subtropical forests along two elevational gradients. CATENA 206, 105525.

Hedley, M.J., Stewart, J., Chauhan, B., 1982. Changes in inorganic and organic soil phosphorus fractions induced by cultivation practices and by laboratory incubations. Soil Sci. Soc. Am. J. 46, 970–976.

Helfenstein, J., Tamburini, F., von Sperber, C., Massey, M.S., Pistocchi, C., Chadwick, O. A., Vitousek, P.M., Kretzschmar, R., Frossard, E., 2018. Combining spectroscopic and isotopic techniques gives a dynamic view of phosphorus cycling in soil. Nat. Commun. 9, 3226.

Holbrook, W.S., Riebe, C.S., Elwaseif, M., Hayes, L.J., Basler-Reeder, K., Harry, D.L., Hopmans, W.J., 2014. Geophysical constraints on deep weathering and water storage potential in the Southern Sierra Critical Zone Observatory. Earth Surf. Proc. Land. 39 (3), 366–380.

Holmgren, G.G., 1967. A rapid citrate-dithionite extractable iron procedure. Soil Sci. Soc. Am. Proc. 31, 210–211.

Hothorn, T., Hornik, K., Zeileis, A., 2006. Unbiased recursive partitioning: a conditional inference framework. J. Comput. Graph. Stat. 15, 651–674.

Hothorn, T., Zeileis, A., 2015. partykit: A modular toolkit for recursive partytioning in R. Mach. Learn. Res. 16 (1), 3905–3909.

Hou, E., Chen, C., Kuang, Y., Zhang, Y., Heenan, M., Wen, D., 2016. A structural equation model analysis of phosphorus transformations in global unfertilized and uncultivated soils. Global Biogeochem. Cycles 30, 1300–1309.

Izquierdo, J.E., Houlton, B.Z., van Huysen, T.L., 2013. Evidence for progressive phosphorus limitation over long-term ecosystem development: examination of a biogeochemical paradigm. Plant Soil 367 (1), 135–147.

Jenny, H., 1994. Factors of Soil Formation: A System of Quantitative Pedology. Courier Corporation.

Johnson, D.W., Cole, D.W., Van Miegroet, H., Horng, F., 1986. Factors affecting anion movement and retention in four forest soils. Soil Sci. Soc. Am. J. 50, 776–783.

Klotzbücher, A., Kaiser, K., Klotzbücher, T., Wolff, M., Mikutta, R., 2019. Testing mechanisms underlying the Hedley sequential phosphorus extraction of soils. J. Plant Nutr. Soil Sci. 182, 570–577.

Lajtha, K., Schlesinger, W.H., 1988. The biogeochemistry of phosphorus cycling and phosphorus availability along a desert soil chronosequence. Ecology 69 (1), 24–39.

Mage, S.M., Porder, S., 2013. Parent material and topography determine soil phosphorus status in the Luquillo Mountains of Puerto Rico. Ecosystems 16, 284–294.

Mehmood, A., Akhtar, M.S., Imran, M., Rukh, S., 2018. Soil apatite loss rate across different parent materials. Geoderma 310, 218–229.

Mix, H.T., Ibarra, D.E., Mulch, A., Graham, S.A., Chamberlain, C.P., 2016. A hot and high Eocene Sierra Nevada. Bulletin 128 (3–4), 531–542.

Morford, S.L., Houlton, B.Z., Dahlgren, R.A., 2011. Increased forest ecosystem carbon and nitrogen storage from nitrogen rich bedrock. Nature 477, 78–81.

Murphy, J., Riley, J.P., 1962. A modified single solution method for the determination of phosphate in natural waters. Anal. Chim. Acta 27, 31–36.

Nakayama, Y., Wade, J., Margenot, A.J., 2021. Does soil phosphomonoesterase activity reflect phosphorus pools estimated by Hedley phosphorus fractionation? Geoderma 401, 115279.

Nanzyo, M., Takahashi, T., Sato, A., Shoji, S., Yamada, I., 1997. Dilute acid-soluble phosphorus in fresh air-borne tephras and fixation with an increase in active aluminum and iron. Soil Sci. Plant Nutr. 43 (4), 839–848.

Nanzyo, M., Yamasaki, S.I., 1998. Phosphorus-bearing Mineral in Fresh, Andesite and Rhyolite Tephras in Northern Part of Japan. Phosphorus Res. Bull. 8, 95–100.

Nesbitt, H.W., Young, G., 1982. Early Proterozoic climates and plate motions inferred from major element chemistry of lutites. Nature 299, 715–717.

O'Geen, A.T., Safeeq, M., Wagenbrenner, J., Stacy, E., Hartsough, P., Devine, S., ... & Bales, R. (2018). Southern Sierra Critical Zone Observatory and Kings River Experimental Watersheds: a synthesis of measurements, new insights, and future directions.

Parfitt, R., 1989. Phosphate reactions with natural allophane, ferrihydrite and goethite. Eur. J. Soil Sci. 40, 359–369.

Pillans, B., 1997. Soil development at snail's pace: evidence from a 6 Ma soil chronosequence on basalt in north Queensland, Australia. Geoderma 80 (1–2), 117–128.

Piper, A.M., Gale, H.S., Thomas, H.E., Robinson, T.W., 1939. Geology and ground-water hydrology of the Mokelumne area, No. 780. US Government Printing Office, California.

Porder, S., Chadwick, O.A., 2009. Climate and soil-age constraints on nutrient uplift and retention by plants. Ecology 90 (3), 623–636.

Porder, S., Ramachandran, S., 2013. The phosphorus concentration of common rocks—a potential driver of ecosystem P status. Plant Soil 367, 41–55.

Rasmussen, C., Dahlgren, R.A., Southard, R.J., 2010. Basalt weathering and pedogenesis across an environmental gradient in the southern Cascade Range, California, USA. Geoderma 154, 473–485.

Rasmussen, C., Matsuyama, N., Dahlgren, R.A., Southard, R.J., Brauer, N., 2007. Soil genesis and mineral transformation across an environmental gradient on andesitic lahar. Soil Sci. Soc. Am. J. 71, 225–237.

Rasmussen, C., Southard, R.J., Horwath, W.R., 2006. Mineral control of organic carbon mineralization in a range of temperate conifer forest soils. Glob. Change Biol. 12, 834–847.

Rasmussen, C., Tabor, N.J., 2007. Applying a quantitative pedogenic energy model across a range of environmental gradients. Soil Sci. Soc. Am. J. 71, 1719–1729.

Rasmussen, C., Throckmorton, H., Liles, G., Heckman, K., Meding, S., Horwath, W., 2018. Controls on soil organic carbon partitioning and stabilization in the California Sierra Nevada. Soil Syst. 2, 41.

R Core Team, 2020. R: A language and environment for statistical computing. R Foundation for Statistical Computing, Vienna, Austria. URL https://www.R-project.org/.

Redel, Y., Cartes, P., Demanet, R., Velásquez, G., Poblete-Grant, P., Bol, R., Mora, M.L., 2016. Assessment of phosphorus status influenced by Al and Fe compounds in volcanic grassland soils. J. Soil Sci. Plant Nutr. 16, 490–506.

Riebe, C.S., Granger, D.E., 2013. Quantifying effects of deep and near-surface chemical erosion on cosmogenic nuclides in soils, saprolite, and sediment. Earth Surf. Proc. Land. 38 (5), 523–533.

Satti, P., Mazzarino, M.J., Roselli, L., Crego, P., 2007. Factors affecting soil P dynamics in temperate volcanic soils of southern Argentina. Geoderma 139, 229–240.

Selmants, P.C., Hart, S.C., 2010. Phosphorus and soil development: Does the Walker and Syers model apply to semiarid ecosystems? Ecology 91, 474–484.

Shoji, S., Nanzyo, M., Dahlgren, R., 1994. Volcanic Ash Soils: Genesis, Properties and Utilization. Elsevier.

Southard, R.J., Southard, S.B., 1987. Sand-sized kaolinized feldspar pseudomorphs in a California Humult. Soil Sci. Soc. Am. J. 51, 1666–1672.

Southard, S.B., Southard, R.J., 1989. Mineralogy and classification of andic soils in northeastern California. Soil Sci. Soc. Am. J. 53, 1784–1791.

Takahashi, T., Dahlgren, R.A., Theng, B.K.G., Whitton, J.S., Soma, M., 2001. Potassium-selective, halloysite-rich soils in volcanic materials from northern California. Soil Sci. Soc. Am. J. 65, 516–526.

Takahashi, T., Dahlgren, R.A., Van Susteren, P., 1993. Clay mineralogy and chemistry of soils formed in volcanic materials in the xeric moisture regime of northern California. Geoderma 59, 131–150.

Stookey, L.L., 1970. Ferrozine–-a new spectrophotometric reagent for iron. Anal. Chem. 42, 779–781.

Tian, Z. (2018). Soil and Weathered Bedrock Evolution along an Elevation Gradient in the Southern Sierra Nevada, California, Ph.D. Dissertation, University of California, Davis.

Tian, Z., Hartsough, P.C., O'Geen, A.T., 2019. Lithologic, climatic and depth controls on critical zone transformations. Soil Sci. Soc. Am. J. 83 (2), 437–447.

Tiessen, H., Moir, J., 1993. Characterization of available P by sequential extraction. Soil Sampling Methods Analysis 7, 5–229.

Tiessen, H., Stewart, J.W.B., Cole, C.V., 1984. Pathways of phosphorus transformations in soils of differing Pedogenesis. Soil Sci. Soc. Am. J. 48, 853–858.

Turrin, B.D., Christiansen, R.L., Clynne, M.A., Champion, D.E., Gerstel, W.J., Patrick Muffler, L.J., Trimble, D.A., 1998. Age of Lassen Peak, California, and implications for the ages of late Pleistocene glaciations in the southern Cascade Range. Geol. Soc. Am. Bull. 110 (7), 931–945.

!"count(.//sb:host[1]//child::*//sb:date)">Turner, B.L., Condron, L.M., Richardson, S. J., Peltzer, D.A., Allison, V.J., . Soil organic phosphorus transformations during pedogenesis. Ecosystems 10, 1166–1181.

Turner, B.L., Engelbrecht, B.M., 2011. Soil organic phosphorus in lowland tropical rain forests. Biogeochemistry 103, 297–315.

Walker, T., Syers, J.K., 1976. The fate of phosphorus during pedogenesis. Geoderma 15, 1–194.

Wahrhaftig, C., 1965. Stepped topography of the southern Sierra Nevada, California. Geol. Soc. Am. Bull. 76 (10), 1165–1190.

Wilson, S.G., Lambert, J.-J., Nanzyo, M., Dahlgren, R.A., 2017. Soil genesis and mineralogy across a volcanic lithosequence. Geoderma 285, 301–312.

Yang, X., Post, W.M., 2011. Phosphorus transformations as a function of pedogenesis: a synthesis of soil phosphorus data using Hedley fractionation method. Biogeosciences 8, 2907–2916.

Zhang, G.L., Pan, J.H., Huang, C.M., Gong, Z.T., 2007. Geochemical features of a soil chronosequence developed on basalt in Hainan Island, China. Revista mexicana de ciencias geológicas 24 (2), 261–269.